Lennard-Jones force field parameters for cyclic alkanes from cyclopropane to cyclohexane

Y. Mauricio Muñoz-Muñoz[a,b], Gabriela Guevara-Carrion[b], Mario Llano-Restrepo[a], Jadran Vrabec*[b]

(a) School of Chemical Engineering, Universidad del Valle, Ciudad Universitaria Melendez, Building 336, Apartado 25360, Cali, Colombia; (b) Thermodynamics and Energy Technology, University of Paderborn, Warburger Straße 100, 33098 Paderborn, Germany.

Abstract

Lennard-Jones (LJ) force field parameters for cyclic alkanes from cyclopropane to cyclohexane are proposed. The molecular geometry is obtained from quantum mechanical calculations. The united-atom approach is applied by initially locating each site at the carbon atom position and subsequently changing the site-site distance; thereby, the LJ parameters and the site-site distance are optimized to vapor-liquid equilibrium (VLE) data, i.e. vapor pressure, saturated liquid density and enthalpy of vaporization. These new cycloalkane force fields are able to describe the VLE data with deviations of a few percent. Furthermore, self-diffusion coefficient, shear viscosity and thermal conductivity are calculated by molecular dynamics simulation and the Green-Kubo formalism. For the smaller two cycloalkanes, i.e. cyclopropane and cyclobutane, the predicted transport properties are in good agreement with the available experimental data. However, the force fields for cyclopentane and cyclohexane specified in this way do not predict transport properties with the desired accuracy. Therefore, they are re-optimized to experimental data on VLE properties and self-diffusion coefficient simultaneously. Then, also the other transport properties meet the experimental data well.

Keywords: cyclopropane, cyclobutane, cyclopentane, cyclohexane, vapor-liquid equilibria, transport properties, molecular simulation, force field

* corresponding author: jadran.vrabec@upb.de

1. Introduction

Molecular modeling and simulation is a powerful approach for studying static and dynamic thermophysical property data. Nowadays, it is widely employed to obtain thermophysical data of condensed phases under conditions which are difficult to handle experimentally. There are thus numerous molecular simulation applications of interest for process engineering, e.g. adsorption equilibria [1], vapor-liquid equilibria (VLE) [2] or chemical equilibria [3].

Cyclic alkanes and their derivatives are important for many chemical engineering applications, especially in the petrochemical and in the resin industries. E.g. napthenes (i.e. cycloalkanes) are dehydrogenated by catalytic reforming to aromatic hydrocarbons, such as benzene, toluene or xylenes [4]. Cyclopentane is used as a blowing agent for polyurethane foams that are employed for thermal insulation purposes, e.g. in domestic refrigerators and freezers [5]. Cyclohexanone, obtained by oxidation of cyclohexane, is converted by means of catalytic oxidation with air into dicarboxylic acids, which are essential raw materials to yield polyesters, polyamides, plasticizers and lubricating oils [6].

On the basis of accurate force fields, molecular simulation may yield thermophysical data for extending equations of state or proposing new ones from hybrid data [7]. To the best of our knowledge, there are no fundamental equations of state reported in the literature for cyclopropane and cyclobutane, because only few experimental data exist due to the poor chemical stability of these compounds. Fundamental equations of state are, however, available for cyclopentane and cyclohexane. The equation for cyclopentane by Gedanitz et al. [8] is valid in the temperature range 179.7–550 K up to a pressure of 250 MPa and a density of 12.11 mol l^{-1}. The equation for cyclohexane by Zhou et al. [9] is valid in the temperature range 279.47–700 K up to a pressure of 250 MPa and a density of 10.30 mol l^{-1}. These fundamental equations of state were used here as a reference to assess the simulation results of the present work.

Force fields consist of molecular geometric structure and interaction parameters. A widely accepted methodological route to devise force fields is to determine the molecular structure, i.e. bond lengths and angles, with quantum mechanical (QM) methods in a first step [10]. Subsequently, the intermolecular interactions are modelled by optimization of the Lennard-Jones (LJ) parameters to experimental VLE data [10-11]. Depending on the importance of conformational changes, the internal degrees of freedom are considered as well, and their parameters are typically transferred from QM calculations too [12-13].

Several force fields for cyclic alkanes are available in the literature. For cyclopropane, Lustig [14] proposed a three center LJ model which was fitted to experimental values for vapor pressure and saturated liquid density at 318.15 K. For the cyclic alkanes cyclobutane to cyclohexane, force fields based on the GROMOS96 family [15] were developed for biomolecular systems. For cyclopentane and cyclohexane, several LJ-based force fields which consider the internal degrees of freedom have been published [16-18]. The TraPPE-UA force fields [16] were fitted to vapor pressure, saturated liquid density and critical temperature. The force fields parameters proposed by Bourasseau et al. [17] were obtained by means of a rigorous optimization procedure, whereas in the work by Neubauer et al. [18] the LJ parameters were fitted to saturated liquid density by means of random search, keeping the bond lengths constant. There are also several rigid force fields for cyclohexane [10, 19-21]. Eckl et al. [10] developed a set of non-polarizable force fields, which included a cyclohexane model. These force fields are based on information from QM calculations to specify geometry and electrostatics, the LJ parameters were fitted to VLE data with a Newton scheme. Errington and Panagiotopoulos [19] proposed a model based on the Buckingham exponential-6 potential, which was optimized to vapor pressure, saturated densities and critical point. The force field by Hoheisel and Würflinger [20] is a LJ-based model which was fitted to reproduce the experimental pressure of liquid and solid states. In case of the all-atom model for cyclohexane by Milano and Müller-Plathe [21], the LJ parameters for carbon and hydrogen were fitted to experimental values of density and enthalpy of vaporization by means of the simplex method.

In this work, the united atom approach was applied to cyclic molecules from cyclopropane to cyclohexane. All molecules were considered as a set of methlylene (CH_2) sites, which are bonded according to their energetically most favorable geometric structure. The molecules are considered as non-polar fluids employing LJ sites only.

Having specified the geometry in terms of the bond angles, there are three parameters that can be fitted for each of the cycloalkane force fields. These are the LJ size and energy parameters for the methylene sites as well as the site-site distance. The site-site distances were varied to account for the absence of the hydrogen molecules following the approach proposed by Toxvaerd [22]. This approach, has been used e.g. by Ungerer et al. [23] and Bourasseau et al. [17] to optimize the Anisotropic United Atoms (AUA) force field family. In this work, the relative magnitude of the site-site distance was kept constant, by taking the results from QM calculations as a starting point. All parameters were subsequently optimized with the reduced

unit method by Merker et al. [24], which does not require additional molecular simulation runs.

The prediction of the transport properties of liquids by molecular simulation is particularly significant, because these data are generally difficult to model accurately, especially with phenomenological approaches. Thus transport properties are considered as a challenging test for force fields. E.g., that predictive task was proposed for mixtures of type water + short alcohol as a benchmark for the development of water models [25]. Therefore, the capability of the present rigid cycloalkane models with respect to the prediction of the most important transport properties, i.e. self-diffusion coefficient, shear viscosity and thermal conductivity, was assessed.

2. Parameterization procedure

The parameterization procedure by Eckl et al. [10] was adapted here. First, the molecular structure of the considered cyclic molecules was determined by means of the open source code for computational chemistry calculations GAMESS (US) [26]. A Hartree-Fock calculation with a relatively small (6–31 G) basis set was chosen to calculate the positions of all carbon and hydrogen atoms.

Next, the united atom approach was applied to the methylene groups that were initially located at the carbon atom positions of molecular structure from QM. Then, the bond angles θ, ϕ and the site-site distances r between the methylene groups were calculated employing the equations reported by Essén and Svensson as implemented in the software EVCLID [27]

$$r(i,j) = \left|\boldsymbol{a}_j - \boldsymbol{a}_i\right|, \tag{1}$$

$$\boldsymbol{b}_{i,j} = \left(\boldsymbol{a}_j - \boldsymbol{a}_i\right)/r(i,j), \tag{2}$$

$$\theta(i,j,k) = \arccos\left(\boldsymbol{b}_{j,i} \cdot \boldsymbol{b}_{j,k}\right), \tag{3}$$

$$\boldsymbol{b}_{i,j,k} = \left(\boldsymbol{b}_{i,j} \times \boldsymbol{b}_{i,k}\right)/\sin[\theta(i,j,k)], \tag{4}$$

$$\phi(i,j,k,l) = \mathrm{sign}\left(\boldsymbol{b}_{i,j} \cdot \boldsymbol{b}_{j,k,l}\right) \cdot \arccos\left(\boldsymbol{b}_{i,j,k} \cdot \boldsymbol{b}_{j,k,l}\right), \tag{5}$$

where the lower indices i, j, k, l represent the methylene sites and $\boldsymbol{a}_i$ represents the position vector of site i. By keeping the bond angles $0 \leq \theta(i,j,k) \leq 180°$ and $-180° \leq \phi(i,j,k,l) \leq 180°$ fixed, the site-site distances $r(i,j)$ were varied by a small quantity dr. The modified Cartesian methylene site coordinates were then recalculated via

$$\begin{aligned} \boldsymbol{r}_n = \boldsymbol{r}_i & \\ & + [r(n,i) \pm dr]\{\cos[\theta(n,i,j)]\boldsymbol{b}_{i,j} \\ & + \sin[\theta(n,i,j)]\left[\cos[\phi(n,i,j,k)]\left(\boldsymbol{b}_{i,j,k} \times \boldsymbol{b}_{i,j}\right)\right. \\ & \left. - \sin[\phi(n,i,j,k)]\boldsymbol{b}_{i,j,k}\right]\}, \end{aligned} \tag{6}$$

where $\boldsymbol{r}_n$ and $\boldsymbol{r}_i$ are the position vectors of sites n and i respectively. $r(n,i) > 0$ is the site-site distance between sites *n* and *i* [27]. One methylene site was assigned to be at the origin of the coordinate system and the positions of other sites were calculated via Eq. (6). Note that the relations between the sometimes different site-site distances remained unchanged.

For each modified geometry, simulation runs were carried out to obtain VLE data with the Grand Equilibrium method [28]. The internal degrees of freedom were neglected, i.e. the molecules were assumed to be rigid structures. The repulsive and dispersive interactions were described by the LJ 12-6 potential model

$$U = \sum_{i=1}^{N-1} \sum_{j=i+1}^{N} \left\{ \sum_{a=1}^{S^{LJ}} \sum_{b=1}^{S^{LJ}} 4\varepsilon \left[\left(\frac{\sigma}{r_{ab,ij}} \right)^{12} - \left(\frac{\sigma}{r_{ab,ij}} \right)^{6} \right] \right\}, \tag{7}$$

where N is the number of molecules in the simulation and S^{LJ} is the number of LJ sites, i.e. three for cyclopropane, four for cyclobutane, five for cyclopentane and six for cyclohexane. σ and ε are the LJ size and energy parameters and $r_{ab,ij}$ is the intermolecular site-site distance between sites a and b of molecules i and j.

Throughout the present work, the LJ parameters of the cyclohexane model by Eckl et al. [10] were taken as a starting point. VLE data were determined with these LJ parameters and the modified geometric structure. Next, the site-site distances were modified, keeping the bond angles constant, until deviations for saturated liquid density and vapor pressure were below 10%. Subsequently, all parameters were optimized with the reduced unit method by Merker et al. [24]. Figure 1 shows the workflow of the implemented parameterization method. Table 1 lists the experimental data selected for the optimization of the force field parameters.

3. Transport properties

The present force fields were assessed with respect to self-diffusion coefficient, shear viscosity and thermal conductivity in the liquid state over a wide range of temperature. The models for cyclopropane and cyclobutane fitted solely to VLE properties were successful in predicting the transport properties, whereas the models for cyclopentane and cyclohexane had to be modified further (see below).

Throughout, equilibrium molecular dynamics (MD) simulation and the Green-Kubo formalism [47] were used to sample transport data. This formalism establishes a direct relationship between a transport coefficient and the time integral of the autocorrelation function of the corresponding microscopic flux in a system in equilibrium.

The Green-Kubo expression for the self-diffusion coefficient D_i is related to the individual molecule velocity autocorrelation function

$$D_i = \frac{1}{3N}\int_0^\infty dt\langle \boldsymbol{v}_i(t)\cdot\boldsymbol{v}_i(0)\rangle, \tag{8}$$

where $\boldsymbol{v}_i(t)$ is the center of mass velocity vector of molecule i at some time t. Eq. (8) is an average over all N molecules in the ensemble, because all contribute to the self-diffusion coefficient. The brackets $\langle\ \ \rangle$ denote the ensemble average.

The shear viscosity is associated with the time autocorrelation function of the off-diagonal elements of the stress tensor $\boldsymbol{J}_p$

$$\eta = \frac{1}{Vk_BT}\int_0^\infty dt\langle J_p^{xy}(t)\cdot J_p^{xy}(0)\rangle, \tag{9}$$

where V stands for the volume, k_B is the Boltzmann constant and T denotes the absolute temperature. The statistics of the ensemble average in Eq. (9) can be improved using all three independent off-diagonal elements of the stress tensor, i.e. J_p^{xy}, J_p^{xz} and J_p^{yz}. For a pure fluid, the component J_p^{xy} of the microscopic stress tensor $\boldsymbol{J}_p$ is given by

$$J_p^{xy} = m\sum_{i=1}^{N} v_i^x v_i^y - \frac{1}{2}\sum_{i=1}^{N}\sum_{j\neq j}^{N}\sum_{a=1}^{S_i}\sum_{b=1}^{S_j} r_{ij}^x \frac{\partial u_{ij}}{\partial r_{ab}^y}, \tag{10}$$

where i and j are the indices of the particles and the lower indices a and b count the interaction sites. The upper indices x and y denote the spatial vector components, e.g. for velocity v_i^x or site-site distance r_{ab}^y.

The thermal conductivity λ is given by the autocorrelation function of the spatial elements of the microscopic heat flow $\boldsymbol{J}_q$

$$\lambda = \frac{1}{Vk_BT^2}\int_0^\infty dt\langle J_q^x(t)\cdot J_q^x(0)\rangle. \tag{11}$$

In analogy to the shear viscosity, statistics can be improved using all three independent elements of the heat flow vector, i.e. J_q^x, J_q^y and J_q^z. The expression for the heat flow $\boldsymbol{J}_q$ for a pure fluid is given by

$$\boldsymbol{J}_q = \frac{1}{2}\sum_{i=1}^{N}\left[\left(m_i\boldsymbol{v}_i^2 + \boldsymbol{w}_i\boldsymbol{I}_i\boldsymbol{w}_i + \sum_{j\neq i}^{N} u_{ij}\right)\cdot\boldsymbol{v}_i\right] - \frac{1}{2}\sum_{i=1}^{N}\sum_{j\neq i}^{N}\sum_{a=1}^{S_i}\sum_{b=1}^{S_j}\boldsymbol{r}_{ij}\cdot\left(\boldsymbol{v}_i\frac{\partial u_{ij}}{\partial \boldsymbol{r}_{ab}} + \boldsymbol{w}_i\boldsymbol{\Gamma}_{ij}\right), \tag{12}$$

where $\boldsymbol{w}_i$ is the angular velocity vector of molecule i and $\boldsymbol{I}_i$ its angular momentum of inertia matrix. u_{ij} is the intermolecular potential energy and $\boldsymbol{\Gamma}_{ij}$ is the torque due to the interaction between molecules i and j.

4. Results and discussion

4.1. Geometric structure

The molecular structure of cyclopropane obtained in this work from QM calculations has bond angles of 60° between the carbon atoms, the C–C distance is 1.503 Å and the C–H distance is 1.084 Å. Relative deviations of these distances with respect to values given by the National Institute of Standards and Technology (NIST) [48] are only 0.2% and 0.1%, respectively. The CH_2–CH_2 site distance, obtained with the present parameterization procedure is about 10% larger than the C–C distance obtained from QM calculations, which is consistent with the findings of Bourasseau et al. [17] that united-atom sites should be located at the geometric center of the molecular group.

Puckered structures were obtained for cyclobutane and cyclopentane from QM calculations. The C–C and C–H distances for cyclobutane were found to be 1.545 and 1.094 Å, respectively, and they deviate from NIST data [48] by 0.6% and 0.2%. The CH_2–CH_2 site distance from the present parameterization procedure is about 20% larger than the C–C distance obtained from QM calculations. The C–C and C–H distances for cyclopentane from QM calculations are 1.541 and 1.096 Å, respectively, and the bond angles are in good agreement with other force fields from the literature [16, 18]. The deviations of the C–C and C–H distances with respect to NIST data [48] are 0.3% and 1.7%, respectively, and the CH_2–CH_2 site distance obtained with the parameterization procedure is about 20% larger than the C–C distance obtained from QM calculations.

For cyclohexane, five molecular configurations are possible: chair, half chair, boat, twist boat I and twist boat II [49]. Chair is the most stable configuration of cyclohexane and nearly all of its derivatives, because it is free of angle and torsional strain [50]. Therefore, it was chosen here. The bending and dihedral angles of 111.17° and 55.59° between the carbon atoms were obtained from QM calculations and are in good agreement with experimental data [51]. The C–C and C–H distances from QM calculations are 1.529 and 1.098 Å, respectively. They compare well with data from NIST [48], the deviations are only 0.04% and 0.1%. The CH_2–CH_2 site distance obtained for cyclohexane with the present parameterization procedure is also about 20% larger than the C–C distance obtained from QM calculations.

Figure 2 represents all geometric structures of the united-atom force fields obtained in this work and Tables 2 and 3 list the parameters from QM calculations and the parameterization procedure outlined in Figure 1.

A comparison with other force field parameters from the literature [10, 14, 16-18, 20] is given in Table 3. For cyclopropane, the site-site distance and the LJ energy parameter ε reported by Lustig [14] are about 12% larger than in case of the present model, whereas the LJ size parameter σ is similar. For cyclobutane, no other force field was found. The force fields for cyclopentane and cyclohexane obtained in this work are in good agreement with those by Bourasseau et al. [17], which take the internal degrees of freedom into account.

4.2. Vapor-liquid equilibria

VLE properties in absolute terms are shown in Figures 3 to 6. In these figures, the solid lines represent the results from fundamental equations of state [8, 9] or empirical correlations by

DIPPR [52]. The experimental values for saturation properties and critical point were taken from the references given in Table 1.

In case of cyclopropane, the vapor pressure was calculated with the DIPPR correlation [52], whereas the enthalpy of vaporization was calculated with the Watson equation [53] on the basis of experimental data by Lin et al. [29]. The saturated liquid density was calculated by means of the Rackett equation [54] ($\rho_L = {z_c}^{-(1-T_r)^n}/v_c$), where ρ_L is the saturated liquid density, z_c is the critical compressibility factor, v_c is the critical volume, T_r is the reduced temperature and the exponent $n = 0.2863$ was optimized to experimental data by Lin et al. [29]. The saturated vapor density for cyclopropane was obtained via the Clausius-Clapeyron equation.

The deviations between the present simulation results and the corresponding fundamental equations of state or DIPPR correlations are shown in Figures 7 to 10. For cyclopropane, the absolute average deviations are 2.6% for vapor pressure, 0.5% for saturated liquid density and 2.2% for enthalpy of vaporization. The model by Lustig [14] exhibits an average deviation of only 0.7% for vapor pressure, but a relatively large average deviation of 2.3% for saturated liquid density. The enthalpy of vaporization was not reported by the author. For cyclobutane, the deviations are 7.2%, 0.5% and 3.3% for vapor pressure, saturated liquid density and enthalpy of vaporization, respectively. No other force fields were found for cyclobutane.

For cyclopentane, with parameters optimized to VLE properties only, the average absolute deviations are 2.7%, 0.9% and 3.4%, respectively; with parameters optimized to VLE and self-diffusion coefficient data, these deviations are 5.7%, 0.3% and 5.9%. For cyclohexane, with parameters optimized to VLE properties only, these deviations are 1.1%, 0.5% and 2.9%, and with parameters optimized to VLE and self-diffusion coefficient data they are 21.7%, 0.7% and 16%. Figure 10 shows a comparison with other cyclohexane simulation results from the literature [10, 16-17, 55]. It can be seen that the present cyclohexane results are similar to those from the literature [10, 17, 55] for the VLE properties. However, the present model optimized solely to VLE properties provides smaller average deviations. E.g. the model by Eckl et al. [10] yields 2.3% for vapor pressure, 0.9% for saturated liquid density and 5.3% for enthalpy of vaporization. The model by Bouresseau et al. [17] yields 5.1%, 3.9% and 2.8% and the model by Merker et al. [55] yields 2.4%, 0.7% and 4.3%. An overview of the average deviations from experiment of the present force fields for vapor pressure, saturated liquid density and enthalpy of vaporization is given in the Supplementary Material.

Table 4 lists the critical data obtained with the present force fields and those of other models from the literature. In this work, all critical data were overestimated, except for the critical density of cyclohexane. For cyclopropane, the deviations in terms of critical temperature, critical pressure and critical density are 1.7%, 5.7% and 2.6%, respectively. In case of cyclobutane, they are 2.2%, 6.4% and 0.8%. For cyclopentane, these deviations are 0.8%, 5% and 2.1%. The deviation of the critical temperature is similar [16-17] or lower[18] than that of other force fields from the literature. The critical pressure was not reported in Refs. [16-18]. The force field by Neubauer et al. [18] reproduces the experimental critical density well and better than other works [16-17]. The critical point of the present cyclohexane model is in good agreement with experimental values. The deviations for the critical temperature, critical pressure and critical density are 0.1%, 0.5% and 0.7%, respectively. Although other force fields [16, 19] reproduce the experimental critical temperature well, the present model exhibits smaller deviations than other force fields [10, 17-18]. The critical pressure was not reported in Refs. [16-18] and the deviation from the present force field is smaller than in case of Refs. [10, 19]. The cyclohexane critical density from the present model is similar to some values [17, 19] and smaller than others [10, 16, 18].

4.3. Second virial coefficient

The second virial coefficient was predicted with the force fields developed in this work. These predictions were made for temperatures between 225 K and 1993 K for cyclopropane, 240 K and 2290 K for cyclobutane, 297.5 K and 2560 K for cyclopentane and 276.7 K and 2500 K for cyclohexane. The calculations were carried out by numerically integrating Mayer's f function. Figure 11 shows the present results in comparison with experimental data according to Table 1 and correlations thereof [52]. The present models are in good agreement with the experimental data and with the DIPPR correlations [52]. A comparison with respect to DIPPR correlation values was carried out. For cyclopropane, the average absolute deviation is 0.06 $l \cdot mol^{-1}$, whereas for cyclobutane, cyclopentane and cyclohexane it is 0.05 $l \cdot mol^{-1}$, 0.04 $l \cdot mol^{-1}$ and 0.14 $l \cdot mol^{-1}$, respectively.

4.4. Transport Properties

Cyclopropane

Transport properties of cyclopropane were predicted in the liquid state for temperatures between 150 K and 318 K. In the temperature range from 150 K to 220 K, self-diffusion coefficient, shear viscosity and thermal conductivity were assessed at ambient pressure, whereas in the temperature range from 250 K to 318 K the saturated liquid state was considered. The numerical simulation results are given in the Supplementary Material. Figure 12 shows that predicted and experimental values for the self-diffusion coefficient are in good agreement with each other. The self-diffusion coefficient was mostly overestimated, the deviations are between 3.5 and 25% with respect to the experimental values. Note that the experimental data themselves exhibit uncertainties of up to 11% [56].

In case of the shear viscosity, Figure 12 shows the present simulation results in comparison with data from correlations [52, 57-58]. Values obtained with the correlation by Liessmann [57] are inconsistent with those from the equations by Rowley et al. [52] and by Yaws [58] for temperatures below 280 K. The present simulations predict shear viscosity data that lie between those obtained from the equations by Rowley et al. [52] and by Yaws [58]. It should be noted that the statistical uncertainties of the simulation results are about 7%, whereas the difference between both predictive equations [52, 58] is mostly below 10%. Since the self-diffusion coefficient was only slightly overestimated, following the Stokes-Einstein relation, the simulation results for the shear viscosity are expected to be slightly underestimated. The present simulation results thus indicate that the equation proposed by Liessmann [57] is inadequate.

Present simulation results for the thermal conductivity are compared in Figure 12 with the correlation by Liessmann [57] and the predictive equations by Rowley et al. [52] and by Yaws [58-59]. Again, the present simulation results are in good agreement with the predictions made with the equation by Rowley et al. [52] within its range of validity. Both correlations by Yaws [58-59] yield comparable results, which are 25 to 30% lower than the results from the equation by Rowley et al. [52]. However, the predictive equation by Liessman [57] leads to thermal conductivity values which are around 20% higher than those predicted with the equation by Rowley et al. [52] and therefore, are also higher than the present results. The large differences among the correlations from the literature can be explained by the lack of

experimental data and the fact that most of the available data are based on estimation methods only.

Cyclobutane

Self-diffusion coefficient, shear viscosity and thermal conductivity were predicted for liquid cyclobutane at temperatures between 220 K and 318.15 K. For temperatures below 285 K, all properties were calculated at 0.1 MPa; otherwise, the vapor pressure was specified. The numerical results are given in the Supplementary Material. To the best of our knowledge, there are no experimental self-diffusion coefficient data; therefore, the present predictions will not be discussed further. In Figure 13, the predicted shear viscosity is compared with correlations [52, 57, 58]. As for cyclopropane, the present results are in good agreement with the equation by Rowley et al. [52], the deviations are below 6.5%. It should be noted that the statistical uncertainties of the simulation results are similar to those deviations, being about 6%. The equation by Yaws [58] predicts values for the shear viscosity that are 20-30% higher than those predicted with the equation by Rowley et al. [52], and are therefore also higher than the present results. On the other hand, at low temperatures, values predicted with the correlation by Liessmann [57] are lower than those predicted with the equation by Rowley et al. [52]; however, both predictions converge for temperatures above 330 K.

The present predictions for the thermal conductivity are shown in Figure 13 in comparison with a single experimental data point and four different predictive equations [52, 57-59]. The simulation results are in good agreement with the equations by Rowley et al. [52] and by Yaws [58], the average deviations are below 6% in both cases. The statistical uncertainties of the simulation results are 5-8%. The experimental data point and the present simulation results invalidate the predictions made with the other correlations [57, 59] that are based on estimation methods.

Cyclopentane

The transport properties predicted with the force field for cyclopentane based on QM calculations and optimized solely to VLE data, show significant deviations; e.g. in the case of the self-diffusion coefficient, the deviations are up to 26%. Dynamics, and hence transport properties, seem to be more sensitive to model simplifications than the static properties. The absence of hydrogen atoms as well the lack of torsional fluctuations, which are more

important for larger molecules [61], result in an overestimation of the self-diffusion coefficient.

Therefore, the force field was re-optimized to describe the self-diffusion coefficient more accurately without significantly compromising the VLE data. The site-site distance was increased to compensate for the implicit hydrogen atoms. This increment leads to larger molecular volumes and therefore, to a decrease in the molecular mobility. As a consequence, the LJ size parameters needed to be reduced, whereas the LJ energy parameters were increased. Figure 14 shows the relative deviation of the self-diffusion coefficient from both force fields and experimental data. As can be seen, the deviation of the self-diffusion coefficient increases with the density. This could be explained because transport properties are very sensitive to the repulsive part of the potential model and less sensitive to the long-range attractive part [61]. Therefore, the effects of the force field simplifications are stronger at low temperatures, resulting in higher deviations from experimental values. Nonetheless, , the relative deviation was substantially reduced, below 15%. In the following, the transport property simulation results for the re-optimized force field are discussed.

Self-diffusion coefficient, shear viscosity and thermal conductivity were sampled for temperatures between 280 K and 318.15 K at 0.1 MPa. For temperatures from 325 K to 348 K, the vapor pressure was specified. The numerical results are given in the Supplementary Material. The self-diffusion coefficient is shown in Figure 15 in comparison with experimental data [63-65] and a correlation [62]. The present simulation results are in good agreement with the experimental data; the average deviation is 4.5% and the maximum deviation is 13%.

Figure 15 shows the predicted shear viscosity of liquid cyclopentane in comparison with experimental data by Ma et al. [66] and various correlations from the literature [52, 58, 62, 67]. The correlation by Lemmon et al. [67] is based on a method proposed by Huber et al. [71]. The present simulation results underestimate the shear viscosity, especially at low temperatures, where the maximum deviation is 17%. This result was expected, because the self-diffusion coefficient was overestimated. Nonetheless, it should be noted that the correlations from the literature differ by up to 20% one from each other.

Present simulation results for the thermal conductivity of liquid cyclopentane are shown in Figure 15 in comparison with experimental data [68-70] and various correlations from the literature [52, 57, 58, 67]. The experimental data and the correlations agree within 10% and

there is a remarkable agreement with the present simulation results, especially for temperatures below 325 K. Note that the statistical uncertainties of the present simulation results are about 5%. Within these uncertainties, the present data match with the correlation by Lemmon et al. [67] almost throughout the entire temperature range.

Cyclohexane

In analogy to cyclopentane, the force field for cyclohexane that was optimized to QM and VLE data only leads to a self-diffusion coefficient that deviates by up to 100% from the experimental data. Therefore, the extended optimization procedure for the site-site distances, that includes the self-diffusion coefficient, was applied to cyclohexane as well. This re-optimized force field reproduces the self-diffusion coefficient with a maximum deviation of 12% in the studied temperature range, cf. Figure 14. Therefore, only the simulation results obtained with the re-optimized force field are discussed in the following.

The numerical simulation results for self-diffusion coefficient, shear viscosity and thermal conductivity of liquid cyclohexane for temperatures from 280 K to 348.15 K at ambient pressure are given in the Supplementary Material. Figure 16 shows the present simulation results for the self-diffusion coefficient in comparison with experimental data [72-77], correlations thereof [62, 78] and other simulation results [21, 79]. It can be seen that the present cyclohexane model is able to describe the self-diffusion coefficient mostly within the scatter of experimental data. Other simulation results [21, 80] using rigid six-site LJ models reported in the literature perform significantly worse than the present model under the studied thermodynamic conditions, cf. Figure 16.

Figure 16 shows the simulation results for the shear viscosity of liquid cyclohexane together with correlations by Rowley et al. [52] and by Lemmon et al. [67]. Other experimental data correlations from the literature are not shown for the sake of clarity, since they are almost identical with the correlations shown here [52, 67]. As expected from the Stokes-Einstein relation, the present simulation data underestimate the shear viscosity with a maximum deviation of 18% at the lowest studied temperature. On the other hand, for temperatures above 320 K, the present simulation results agree with the experimental data correlations within their statistical uncertainties of about 6%. The predicted thermal conductivity of liquid cyclohexane is shown in Figure 16 in comparison with experimental data [81-86] and correlations by Rowley et al. [52], Liessmann [57], Yaws [58] and Lemmon et al. [67]. There is a general trend of the present predictions to overestimate the thermal conductivity

throughout the studied temperature range, with deviations between 10 and 20% from the correlation by Rowley et al. [52], cf. Figure 16. The correlations differ from each other by up to 7%, which can be explained by the scatter of the available experimental data. Present statistical simulation uncertainties are typically about 5%.

5. Conclusions

A set of rigid, non-polarizable united atom force fields for cyclopropane, cyclobutane, cyclopentane and cyclohexane was proposed. These force fields were developed using QM methods and optimization of the site-site distance and LJ parameters to vapor-liquid equilibrium (VLE) data, i.e. vapor pressure, saturated liquid density and enthalpy. This optimization procedure has led to force fields than can describe the experimental VLE properties of the pure substances within a few percent. The VLE data and critical properties obtained using these simple force fields show that at least the same accuracy than computationally more expensive force fields, e.g. those that take into account explicitly hydrogen atoms and/or internal degrees of freedom. Furthermore, the second virial coefficient was successfully predicted for all the force fields by numerically integrating Mayer's f function.

However, a successful optimization of the VLE properties does not guarantee a correct description of the dynamics, therefore the self-diffusion coefficient, shear viscosity and thermal conductivity of the four cyclic alkanes were studied for a wide range of thermodynamic conditions in the liquid state with the present force fields. For this purpose, the Green-Kubo formalism was employed. In case of the smaller cyclic alkanes cyclopropane and cyclobutane, the predicted transport properties for the force fields parameterized using QM and VLE data only agree very well with experimental data and the correlations proposed by Rowley et al. [50] where available. Average deviations from experimental transport data are mostly below 10%.

The predictions of the static and dynamic properties for the smaller cycloalkanes are of great importance because of the lack of experimental data and the existence of contradictory predictive correlations. In case of transport properties, present simulation results evidenced the inadequacy of some empirical correlations based on estimation methods proposed in the literature.

On the other hand, the force fields for the larger molecules cyclopentane and cyclohexane were not able to predict the transport properties with an acceptable accuracy when parameterized to QM and VLE data only mainly because of force field simplifications. As a result, both force fields were re-parameterized increasing the site-site distances to lower the molecular mobility and approximate the experimental self-diffusion coefficient data. These re-optimized force fields are able to reproduce self-diffusion coefficient, shear viscosity and thermal conductivity with deviations usually below 20% in the studied temperature range without strongly compromising the VLE data.

Acknowledgment

Y.M. Muñoz-Muñoz gratefully acknowledges financial support from COLCIENCIAS (Colombian Administrative Department for Science, Innovation and Technology) during his international doctoral research internship at the University of Paderborn. We also acknowledge financial support by BMBF for the project “SKASIM: Skalierbare HPC-Software für molekulare Simulationen in der chemischen Industrie” under the grant H13005G, computational support by the High Performance Computing Center Stuttgart (HLRS) and the help of Andreas Köster during the simulation runs.

Appendix: Simulation details

All VLE, transport property and second virial coefficient calculations were carried out with the *ms*2 program [87]. For the VLE simulations, the Grand Equilibrium method [28] was used. To determine the chemical potential in the liquid phase, Widom’s test molecule method was applied to MD simulations of the liquid phase. The simulated volume contained 500 molecules throughout. The MD simulations started from a face centered cubic lattice and were equilibrated during 70,000 time steps with the initial 20,000 steps in the canonical (NVT) ensemble. The number of production time steps was 300,000 with a time step interval of 3.29 fs. The numerical integration was carried out with Gear’s predictor-corrector method. The chemical potential was determined by inserting 2000 test molecules each time step. For the corresponding simulation in the vapor phase, the volume was adjusted to lead to an average between 300 and 500 molecules. 10,000 initial NVT Monte Carlo cycles, starting

from a cubic face-centered lattice, and 15,000 pseudo-μVT ensemble cycles were carried out for equilibration. The length of the production runs was 150,000 cycles.

MD simulations for transport properties were carried out in two steps. First, a short simulation of 300,000 time steps in the isobaric-isothermal (NpT) ensemble was performed at the chosen temperature and pressure to determine the density. Second, a simulation in the NVT ensemble was performed at this temperature and density to sample the transport properties. The simulations were carried out in a cubic volume with periodic boundary conditions containing 2048 molecules. The temperature was controlled by velocity scaling [88]. The integration time step was 0.98 fs. The cut-off radius was set to r_c = 21 Å. Electrostatic long-range corrections were applied by using the reaction field technique with conducting boundary conditions ($\varepsilon_{RF} = \infty$). On the basis of a center of mass cut-off scheme, the LJ long-range interactions were corrected using angle averaging [89]. The simulations were equilibrated in the NVT ensemble over $3 \cdot 10^5$ time steps, followed by production runs of 4.5 to $9 \cdot 10^6$ time steps. Self-diffusion coefficient, shear viscosity and thermal conductivity were calculated using Eqs. (8) to (12) with up to 44,000 independent time origins of the autocorrelation functions. The sampling length of the autocorrelation functions varied between 10 and 18 ps, depending on the state point. The separation between time origins was chosen such that all autocorrelation functions have decayed at least to 1/e of their normalized value to guarantee their time independence [90]. The uncertainties of the predicted values were estimated with a block averaging method [91].

Tables

Table 1. References for experimental data on vapor-liquid equilibrium properties and second virial coefficient.

	Vapor pressure		Saturated liquid density		Enthalpy of vaporization		Second virial coefficient		Critical point
Substance	*T* / K	Ref.	*T* / K	Ref.	*T* / K	Ref.	*T* / K	Ref.	Ref.
Cyclopropane	293.15–398.3	[29]	293.15–398.3	[29]	293.15–398.3	[29]	198.9–1989	[30]	[29]
							303.15–403.15	[31]	
Cyclobutane	235.65–286.23	[32]	288.71	[33]	182.48–413.94	[34]	230–2300	[30]	[33][a]
	204.52–460	[30]	293.15, 298.15	[30]					
			268.15	[35]					
			293.15	[36]					
Cyclopentane	193–510	[37]	193–510	[37]	193–510	[37]	255.8–2558	[30]	[8]
							298.15–322.41	[38]	
Cyclohexane	451.40–553.60	[39]	280.15–353.15	[40]	353.15–543.15	[41]	276.70–2767	[30]	[9]
	323.15–423.15	[42]	403.15–529.15	[43]	475.37–537.04	[44]			
	383.15–553.50	[45]	301.15–343.15	[46]	279.69–498.22	[34]			

[a] The critical point of cyclobutane was predicted.

Table 2. Site-site distances and bond angles of cycloalkanes obtained by QM calculations.

S_n	i	$r(n,i)$ / Å	j	$\theta(n,i,j)$ / °	k	$\phi(n,i,j,k)$ / °
Cyclopropane						
S_2	1	1.503				
S_3	2	1.503	1	60		
Cyclobutane						
S_2	1	1.545				
S_3	2	1.545	1	87.91		
S_4	3	1.545	2	87.91	1	–21.63
Cyclopentane						
S_2	1	1.53				
S_3	2	1.53	1	102.45		
S_4	3	1.54	2	103.90	1	41.18
S_5	4	1.552	3	105.68	2	–25.36
Cyclohexane						
S_2	1	1.529				
S_3	2	1.529	1	111.17		
S_4	3	1.529	2	111.17	1	–55.59
S_5	4	1.529	3	111.17	2	55.59
S_6	5	1.529	4	111.17	3	–55.59

Table 3 Present force field parameters of the methylene (CH_2) sites obtained with the workflow shown in Figure 1. Other force field parameters from the literature are listed for comparison.

Substance	Ref.	ε/k_B / K	σ / Å	r / Å
Cyclopropane	This work	87.149	3.567	1.686
	[14]	97.96	3.538	1.87514
Cyclobutane	This work	89.050	3.537	1.881
Cyclopentane	This work	88.401	3.506	1.904, 1.904, 1.915, 1.927 [a]
	This work[b]	122.75	3.235	2.219, 2.219, 2.230, 2.242[a]
	[16][c]	56.3	3.88	
	[17][c]	90.09	3.461	1.871
	[18]	50.37 / 50.5	3.93 / 3.85	1.529
Cyclohexane	This work	87.009	3.497	1.904
	This work[b]	147.03	3.095	2.356
	[10][d]	87.39	3.497	
	[16][c]	52.5	3.91	
	[17][c]	90.09	3.461	1.871
	[18]	50.37 / 50.5	3.93 / 3.85	1.532
	[20]	78	3.86	1.78

[a] Distances correspond to those between sites 1–2, 2–3, 3–4 and 4–5, respectively.

[b] Parameters used for assessing transport properties.

[c] Force fields with internal degrees of freedom.

[d] Force field with quadrupolar interaction site.

Table 4. Critical point from the present force fields compared with experimental data as given in Table 1 and with that of other force fields from the literature.

Substance	Ref.	T_c / K	p_c / MPa	ρ_c / mol l^{-1}
Cyclopropane	Exp	398.3	5.5795	6.1431
	This work	405±4.1	5.9±0.35	6.3±0.19
Cyclobutane	Exp[a]	459.93	4.98	4.7619
	This work	470±4.7	5.3±0.32	4.8±0.14
Cyclopentane	Exp	511.72	4.5712	3.82
	This work	516±5.2	4.8±0.29	3.9±0.12
	[16]	515.4±2.7		4.029±0.06
	[17]	507±5		3.921±0.14
	[18]	477±10		3.821±0.4
Cyclohexane	Exp	553.6	4.0805	3.224
	This work	554±5.5	4.1±0.25	3.2±0.10
	[10]	556	4.23	3.26
	[16]	553.8±3.3		3.402±0.05
	[17]	559±5		3.22±0.12
	[18]	532±10		3.672±0.4
	[19]	553.8±0.4	4.21±0.03	3.241±0.01

[a] The critical point of cyclobutane was predicted.

Figure captions

Figure 1 Workflow of the present force field parameterization process.

Figure 2 Molecular structure of the cyclic alkane models developed in the present work: (a) cyclopropane, (b) cyclobutane, (c) cyclopentane and (d) cyclohexane. The diameter of the spheres corresponds to their Lennard-Jones size parameter σ.

Figure 3 Vapor pressure of cycloalkanes. Present molecular simulation results for cyclopropane (△), cyclobutane (◇), cylopentane (○) and cyclohexane (□) are compared with experimental data according to Table 1 (+). Solid lines correspond to calculations as explained in section 4.3.

Figure 4 Clausius-Clapeyron plot of cycloalkanes. Present molecular simulation results for cyclopropane (△), cyclobutane (◇), cylopentane (○) and cyclohexane (□) are compared with experimental data according to Table 1 (+). Solid lines correspond to calculations as explained in section 4.3.

Figure 5 Saturated densities of cycloalkanes. Present molecular simulation results for cyclopropane (△), cyclobutane (◇), cylopentane (○) and cyclohexane (□) are compared with experimental data according to Table 1 (+). Solid lines correspond to calculations as explained in section 4.3.

Figure 6 Enthalpy of vaporization of cycloalkanes. Present molecular simulation results for cyclopropane (△), cyclobutane (◇), cylopentane (○) and cyclohexane (□) are compared with experimental data according to Table 1 (+). Solid lines correspond to calculations as explained in section 4.3.

Figure 7 Relative deviations of vapor-liquid equilibrium properties of cyclopropane from the correlations listed in section 4.3 ($\delta z = (z - z_{corr})/z_{corr}$). Present simulation results (△) are compared with simulation data [14] (▲) and experimental data according to Table 1 (+).

Figure 8 Relative deviations of vapor-liquid equilibrium properties of cyclobutane from the correlations listed in section 4.3 ($\delta z = (z - z_{corr})/z_{corr}$). Present simulation results (◇) are compared with experimental data according to Table 1 (+).

Figure 9 Relative deviations of vapor-liquid equilibrium properties of cyclopentane from a fundamental equation of state [8] ($\delta z = (z - z_{EOS})/z_{EOS}$). Present simulation results (○) are

compared with other simulation data [16] (■) and [17] (●) and experimental data according to Table 1 (+).

Figure 10 Relative deviations of vapor-liquid equilibrium properties of cyclohexane from a fundamental equation of state [9] ($\delta z = (z - z_{EOS})/z_{EOS}$). Present simulation results (□) are compared with other simulation data [10] (■), [16] (▽), [17] (●) and [55] (▲) and experimental data according to Table 1 (+).

Figure 11 Second virial coefficient of cycloalkanes. **a)** Present molecular simulation results for cyclopropane (△) and cyclobutane (◇) and **b)** for cyclopentane (○) and cyclohexane (□) are compared with experimental data according to Table 1 (+) and correlations of experimental data [52] (–).

Figure 12 a) Temperature dependence of the self-diffusion coefficient of liquid cyclopropane. Present simulation results (●) are compared with experimental data [53] (+). The statistical uncertainties of the present simulation results are within symbol size. **b)** Temperature dependence of the shear viscosity of liquid cyclopropane. Present simulation results (●) are compared with correlations [50] (-), [57] (-..-) and [58] (--). **c)** Temperature dependence of the thermal conductivity of liquid cyclopropane. Present simulation results (●) are compared with correlations [52] (-), [57] (-..-), [58] (--) and [59] (-.-). In all subfigures, the pressure is 0.1 MPa for T < 250 K and the vapor pressure otherwise.

Figure 13 a) Temperature dependence of the shear viscosity of liquid cyclobutane. Present simulation results (●) are compared with correlations [50] (-), [57] (-.-) and [58] (--). **b)** Temperature dependence of the thermal conductivity of liquid cyclobutane. Present simulation results (●) are compared with experimental data [60] (+) and correlations [52] (-), [57] (-.-), [58] (--) and [59] (-..-). In all subfigures, the pressure is 0.1 MPa for T < 285 K and the vapor pressure otherwise.

Figure 14 Relative deviations of the self-diffusion coefficient of liquid cyclopentane and cyclohexane from a correlation of experimental data [62]. Simulation results for the force fields optimized to QM and VLE data only for cyclopentane (○) and cyclohexane (□). The solid symbols represent data for the re-optimized models. The statistical uncertainties are within the symbol size.

Figure 15 a) Temperature dependence of the self-diffusion coefficient of liquid cyclopentane. Present simulation results (●) are compared with experimental data [63-65] (+) and a

correlation [62] (-). The statistical uncertainties of the present simulation results are within symbol size. **b)** Temperature dependence of the shear viscosity of liquid cyclopentane. Present simulation results (●) are compared with experimental data [66] and correlations [52] (-), [58] (--), [62] (-..-) and [67] (-.-). **c)** Temperature dependence of the thermal conductivity of liquid cyclopentane. Present simulation results (●) are compared with experimental data [68-70] (+) and correlations [52] (-), [57] (-.-), [58] (--) and [67] (-..-). In all subfigures, the pressure is 0.1 MPa for $T < 325$ K and the vapor pressure otherwise.

Figure 16 a) Temperature dependence of the self-diffusion coefficient of liquid cyclohexane at 0.1 MPa. Present simulation results (●) are compared with experimental data [72-77] (+), correlations [62] (-) and [78] (--) and other simulation results [21] (◇) and [79] (□). The statistical uncertainties of the present simulation results are within symbol size. **b)** Temperature dependence of the shear viscosity of liquid cyclohexane at 0.1 MPa. Present simulation results (●) are compared with correlations [52] (-) and [67] (--). **c**) Temperature dependence of the thermal conductivity of liquid cyclohexane at 0.1 MPa. Present simulation results (●) are compared with experimental data [80-87] (+) and correlations [52] (-), [55] (-.-), [56] (--) and [64] (-..-).

Figure 1.

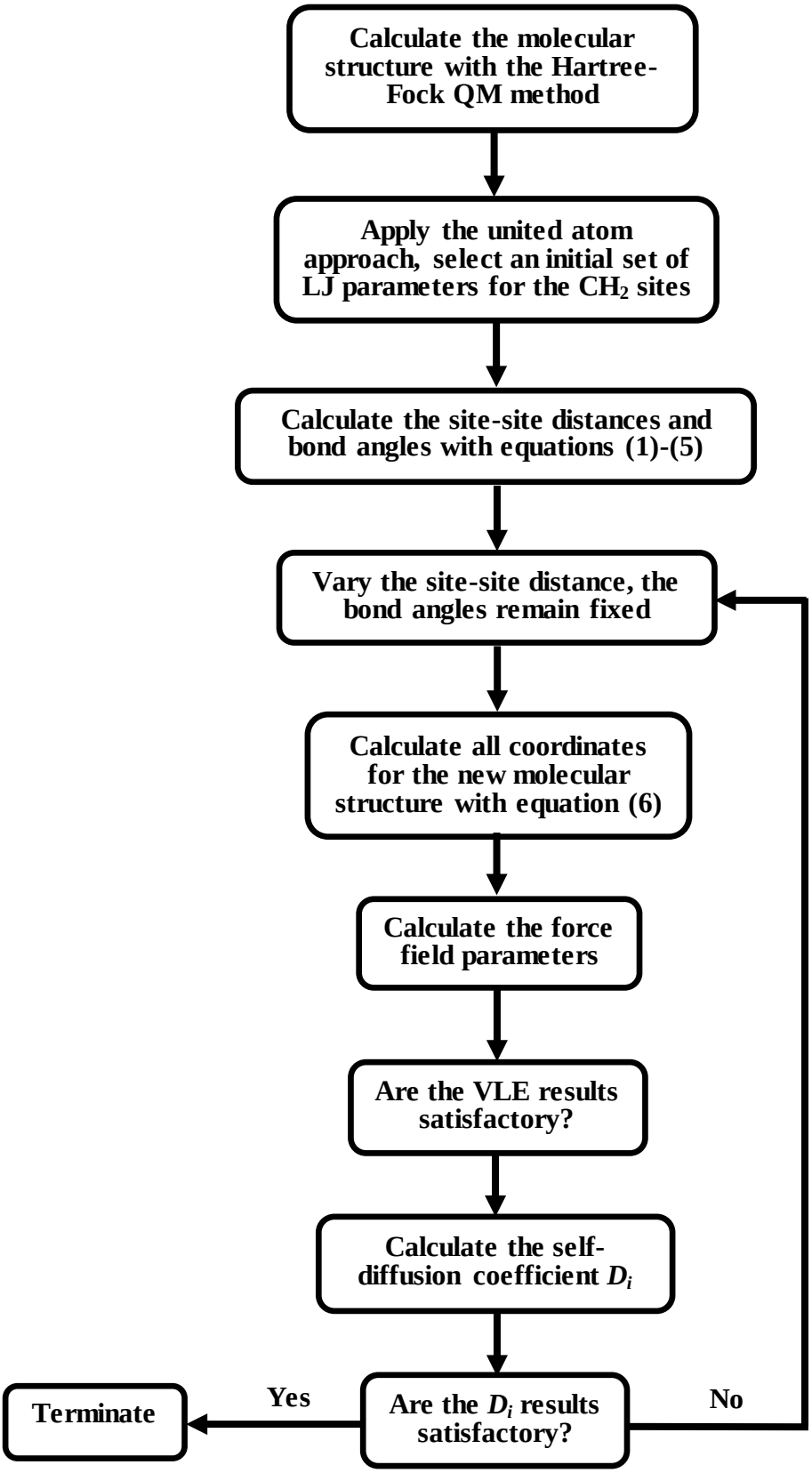
Calculate the molecular structure with the Hartree-Fock QM method
Apply the united atom approach, select an initial set of LJ parameters for the CH_2 sites
Calculate the site-site distances and bond angles with equations (1)-(5)
Vary the site-site distance, the bond angles remain fixed
Calculate all coordinates for the new molecular structure with equation (6)
Calculate the force field parameters
Are the VLE results satisfactory?
Calculate the self-diffusion coefficient D_i
Are the D_i results satisfactory?
Yes
No
Terminate

Figure 2.

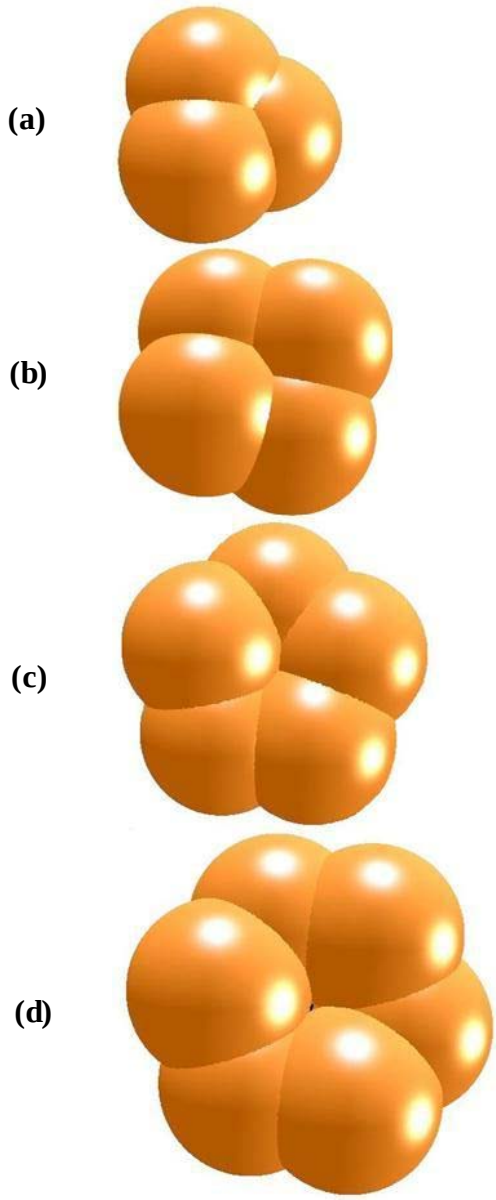

Figure 3.

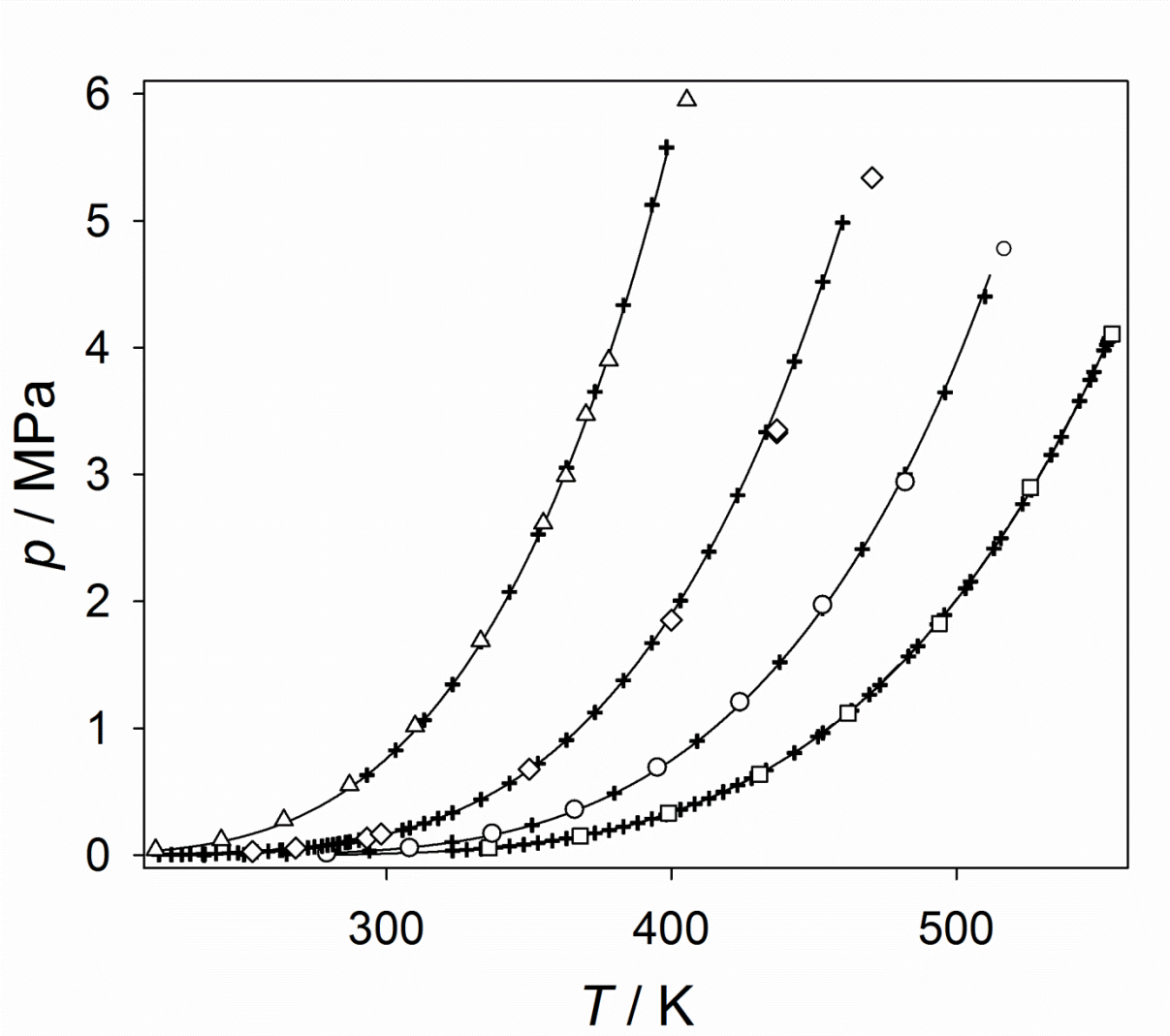

Figure 4.

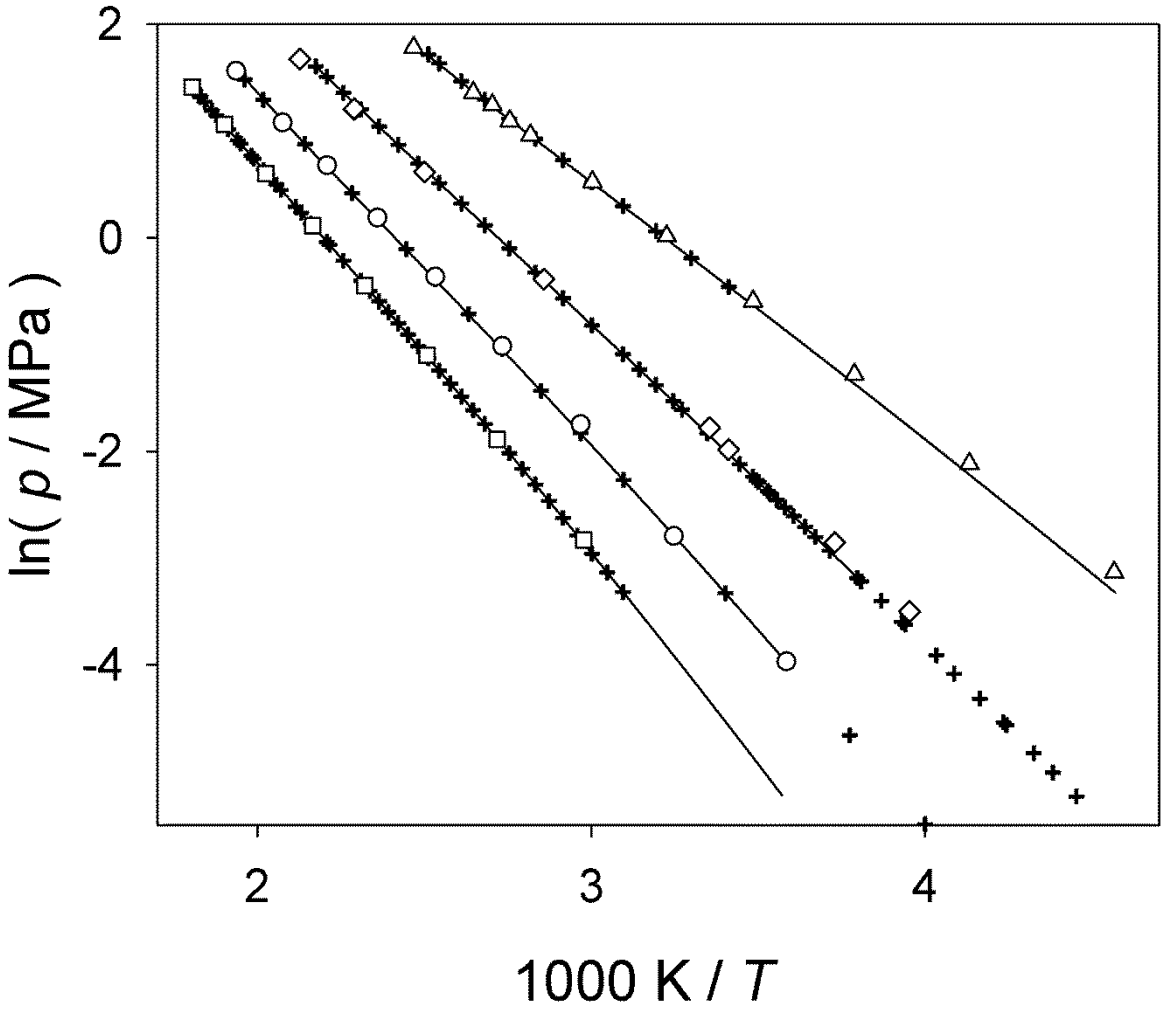

Figure 5.

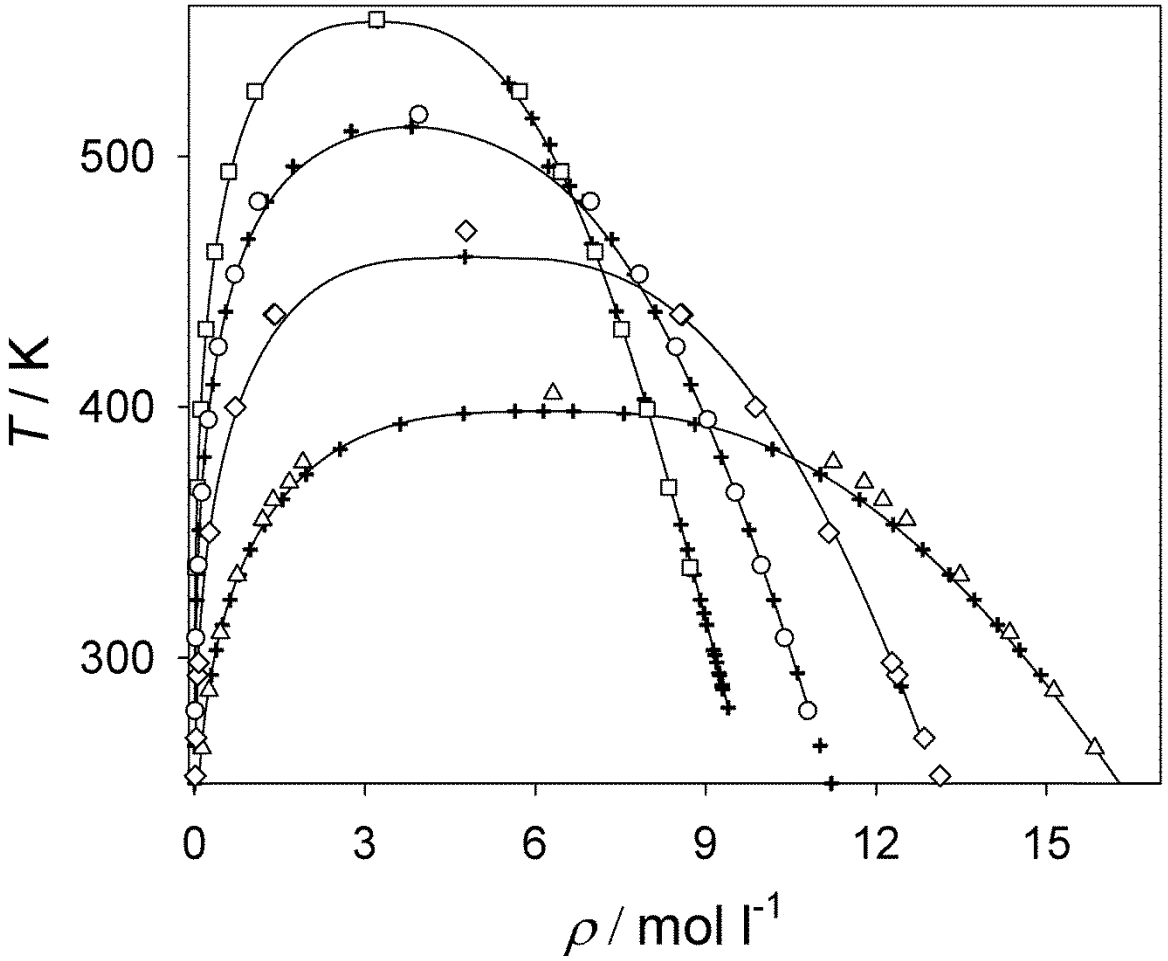

Figure 6.

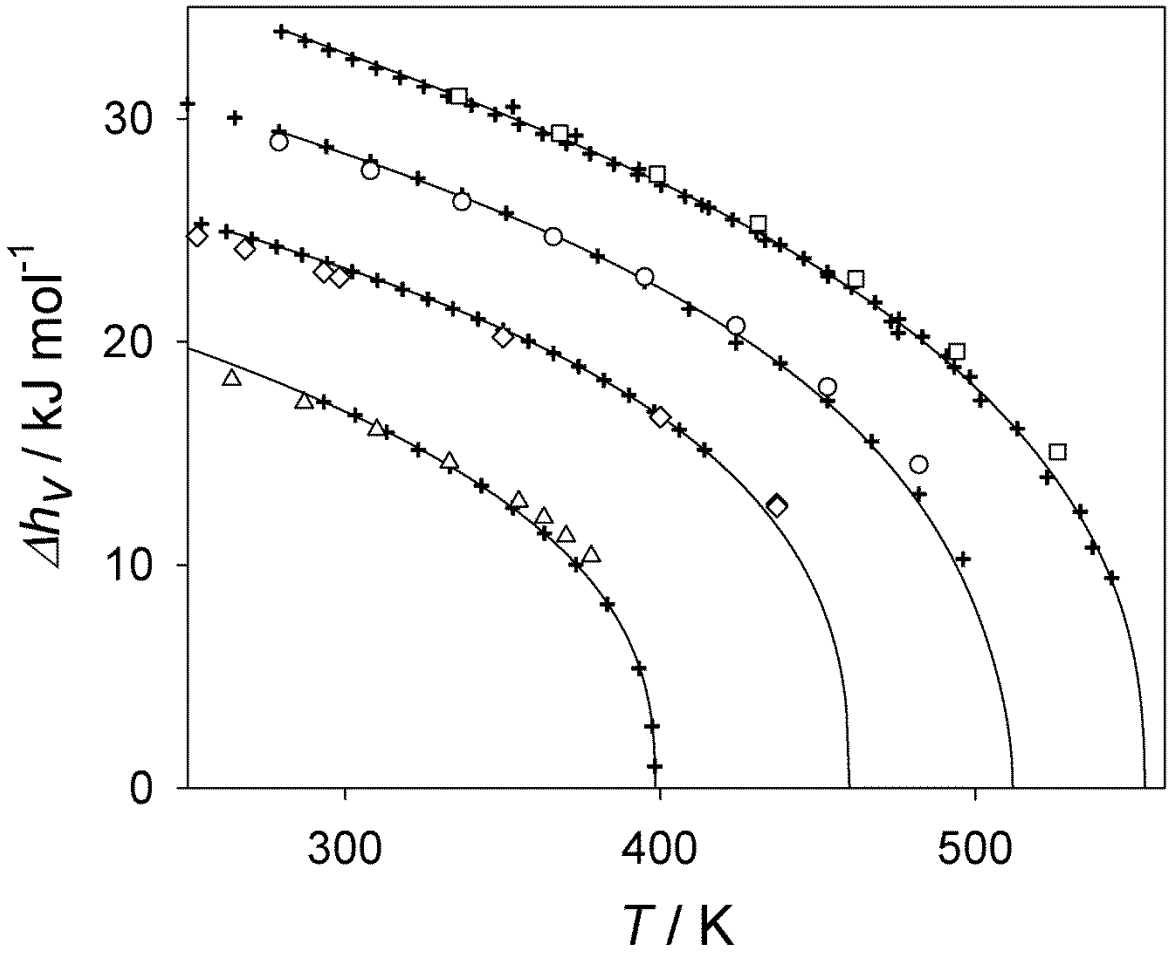

Figure 7.

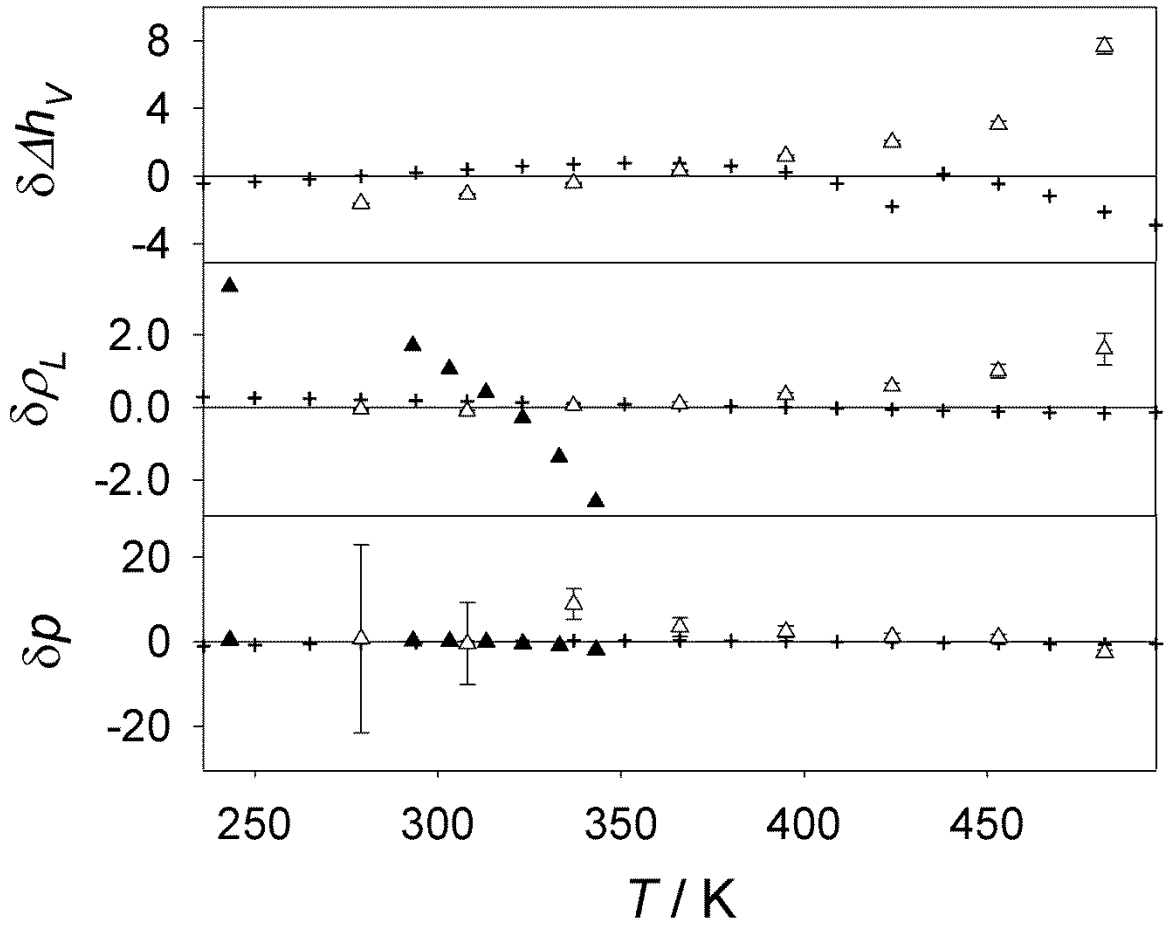
8
4
0
-4
$\delta\Delta h_V$
2.0
0.0
-2.0
$\delta\rho_L$
20
0
-20
δp
250
300
350
400
450
T / K

Figure 8.

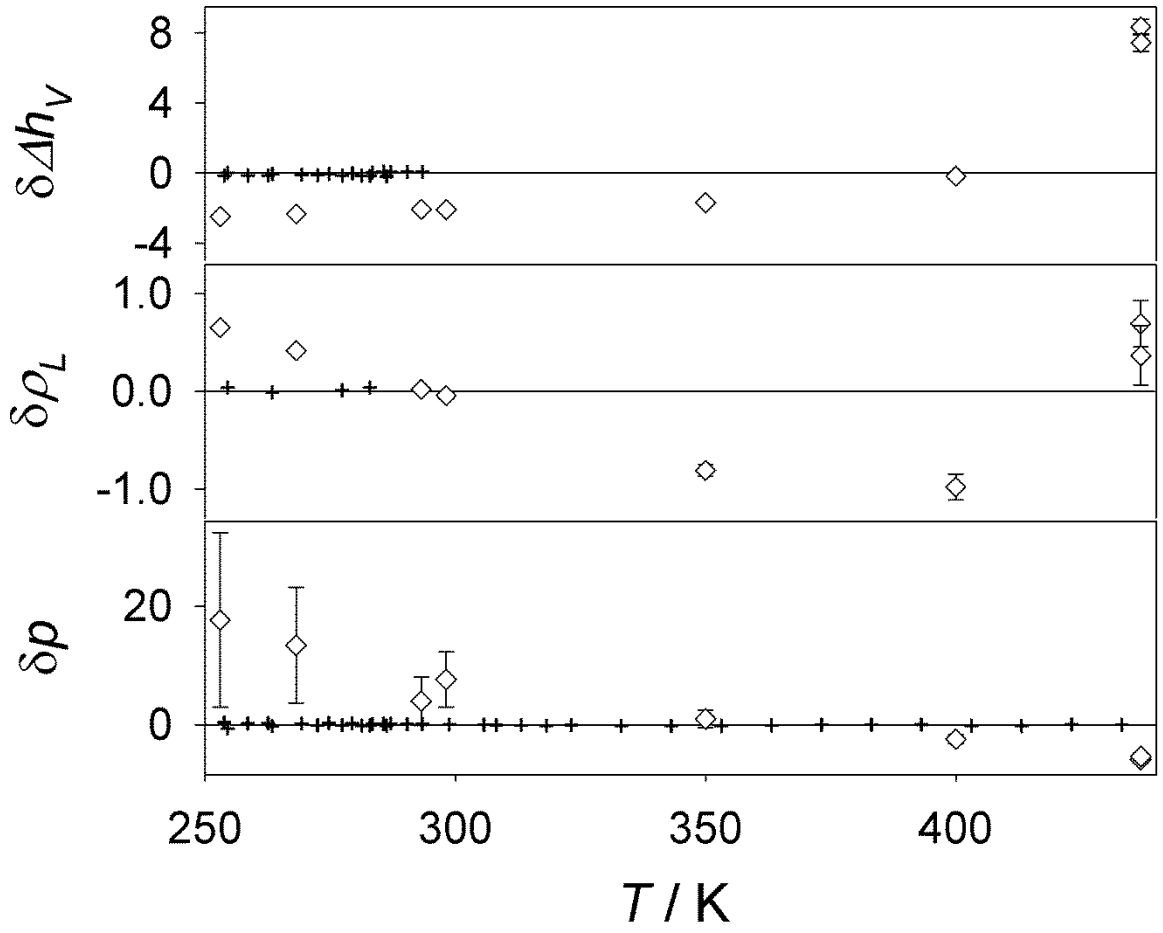

Figure 9.

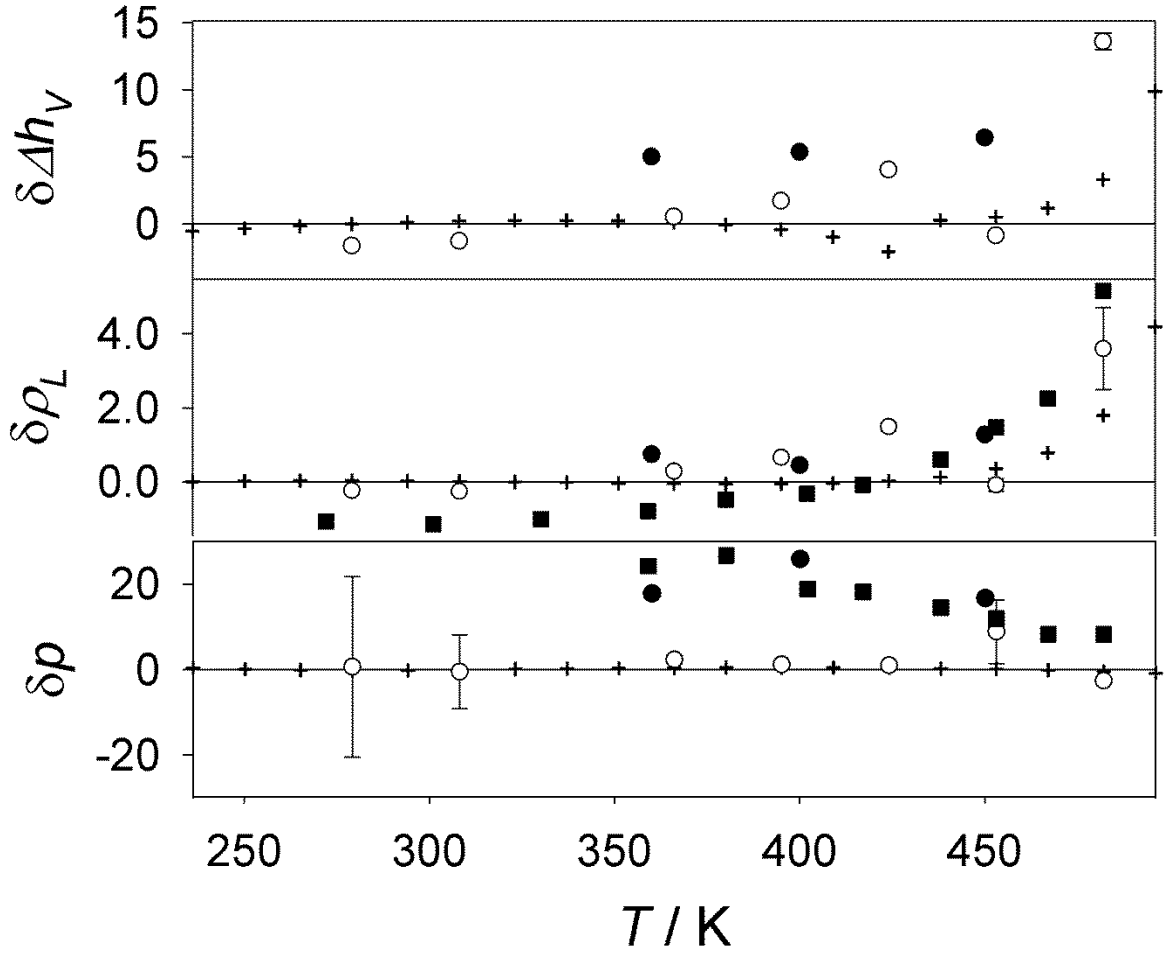
15
10
5
0
$\delta\Delta h_V$
4.0
2.0
0.0
$\delta\rho_L$
20
0
-20
δp
250
300
350
400
450
T / K

Figure 10.

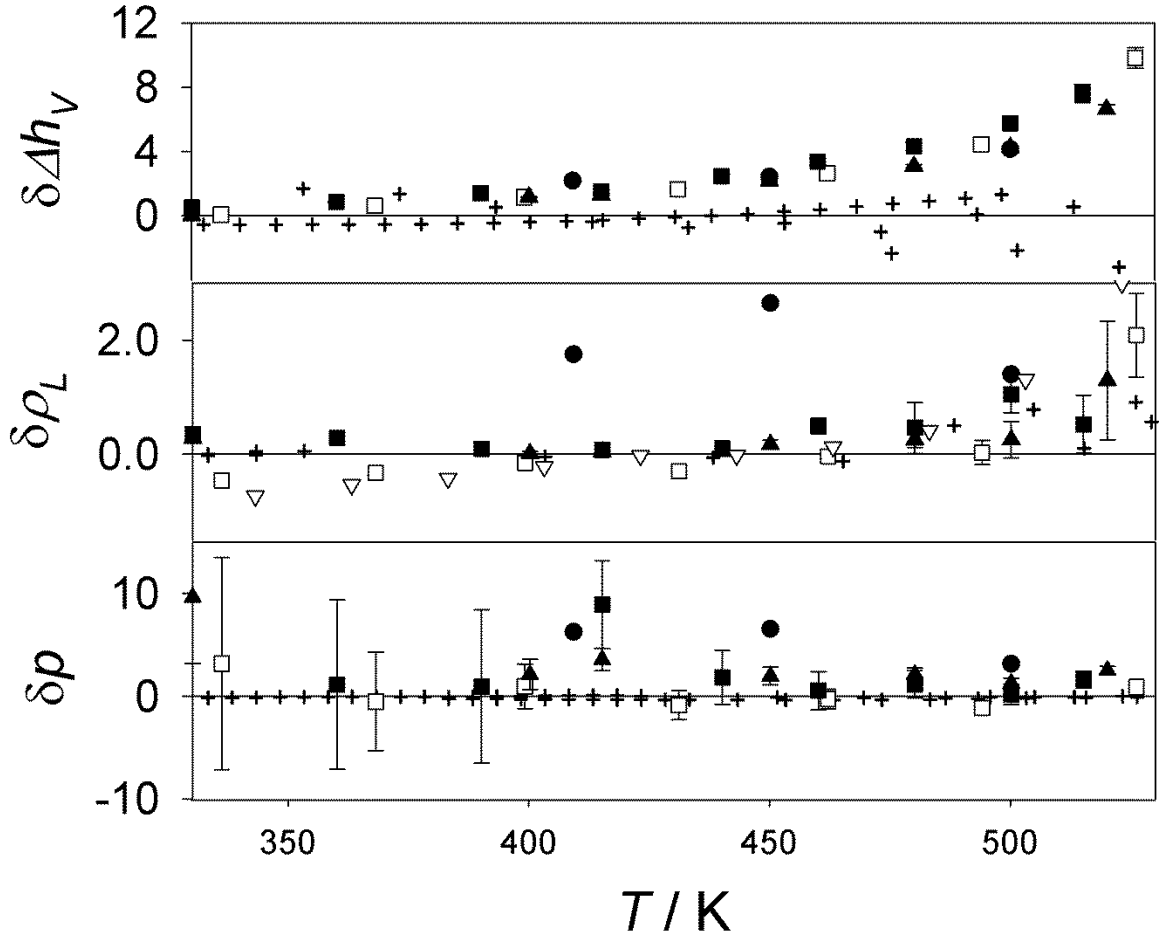
12
8
4
0
$\delta\Delta h_V$
2.0
0.0
$\delta\rho_L$
10
0
-10
δp
350
400
450
500
T / K

Figure 11.

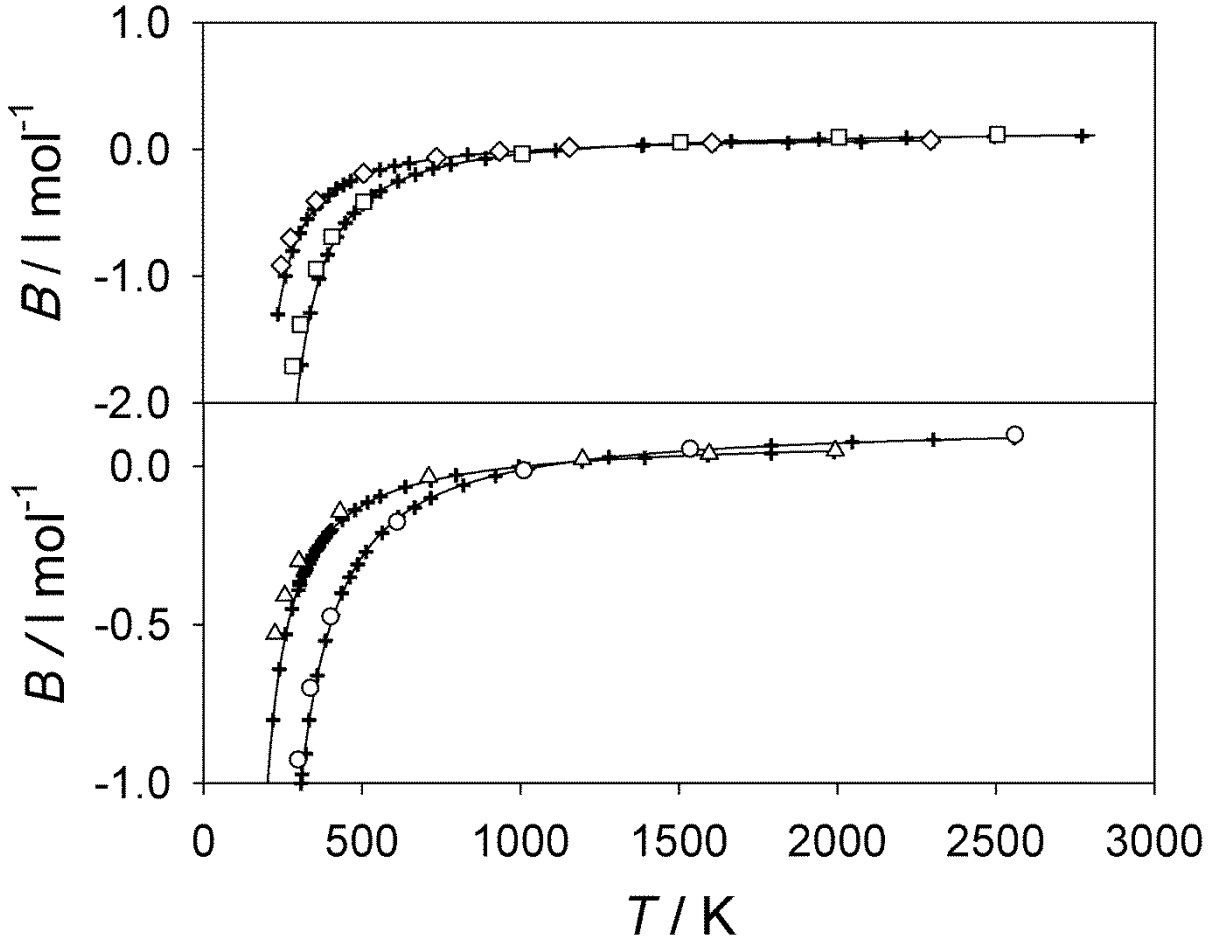
1.0
0.0
-1.0
-2.0
B / l mol-1
0.0
-0.5
-1.0
B / l mol-1
0
500
1000
1500
2000
2500
3000
T / K

Figure 12.

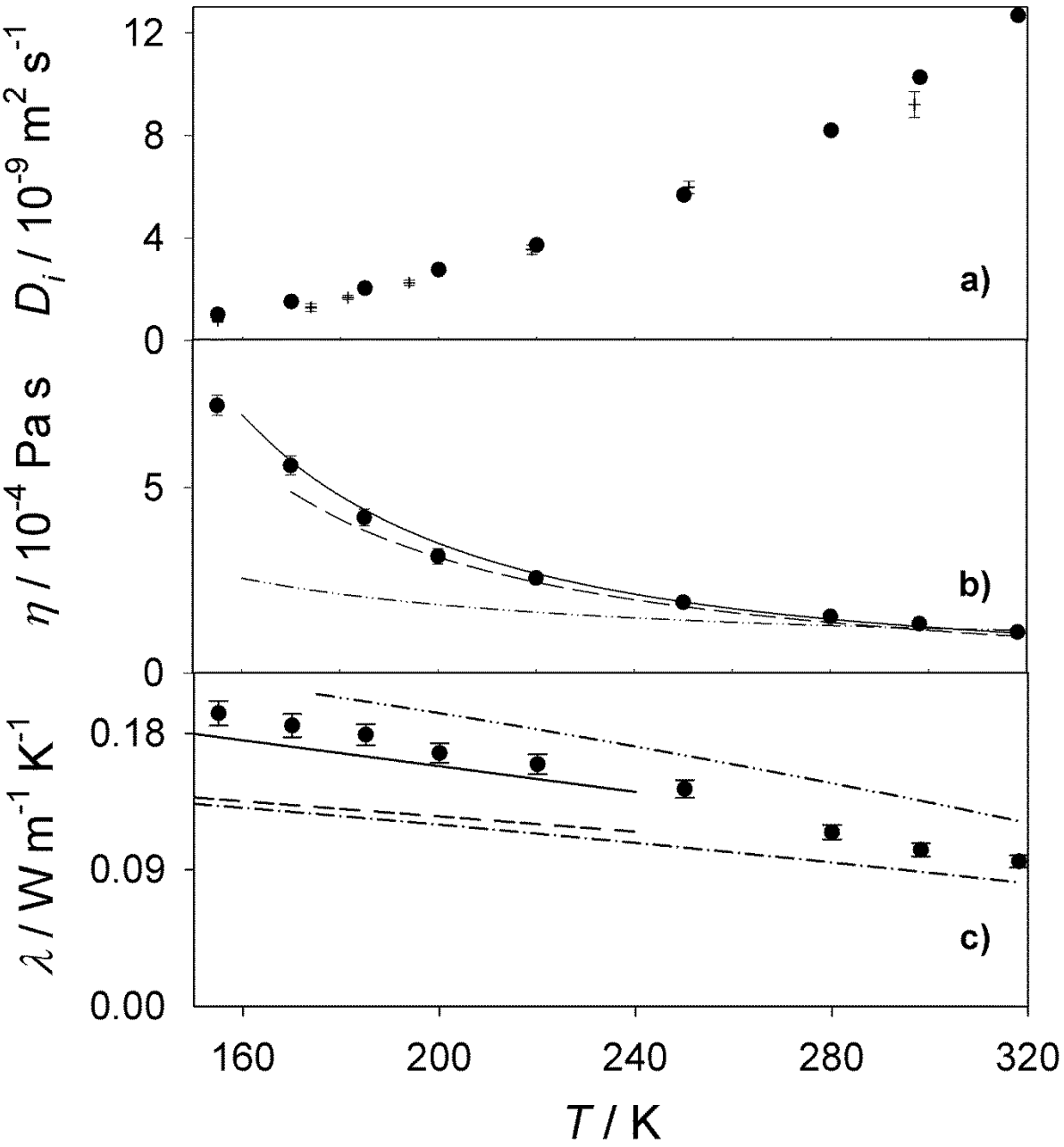
12
8
4
0
D_i / 10^{-9} m^2 s^{-1}
a)
5
0
η / 10^{-4} Pa s
b)
0.18
0.09
0.00
λ / W m^{-1} K^{-1}
c)
160
200
240
280
320
T / K

Figure 13.

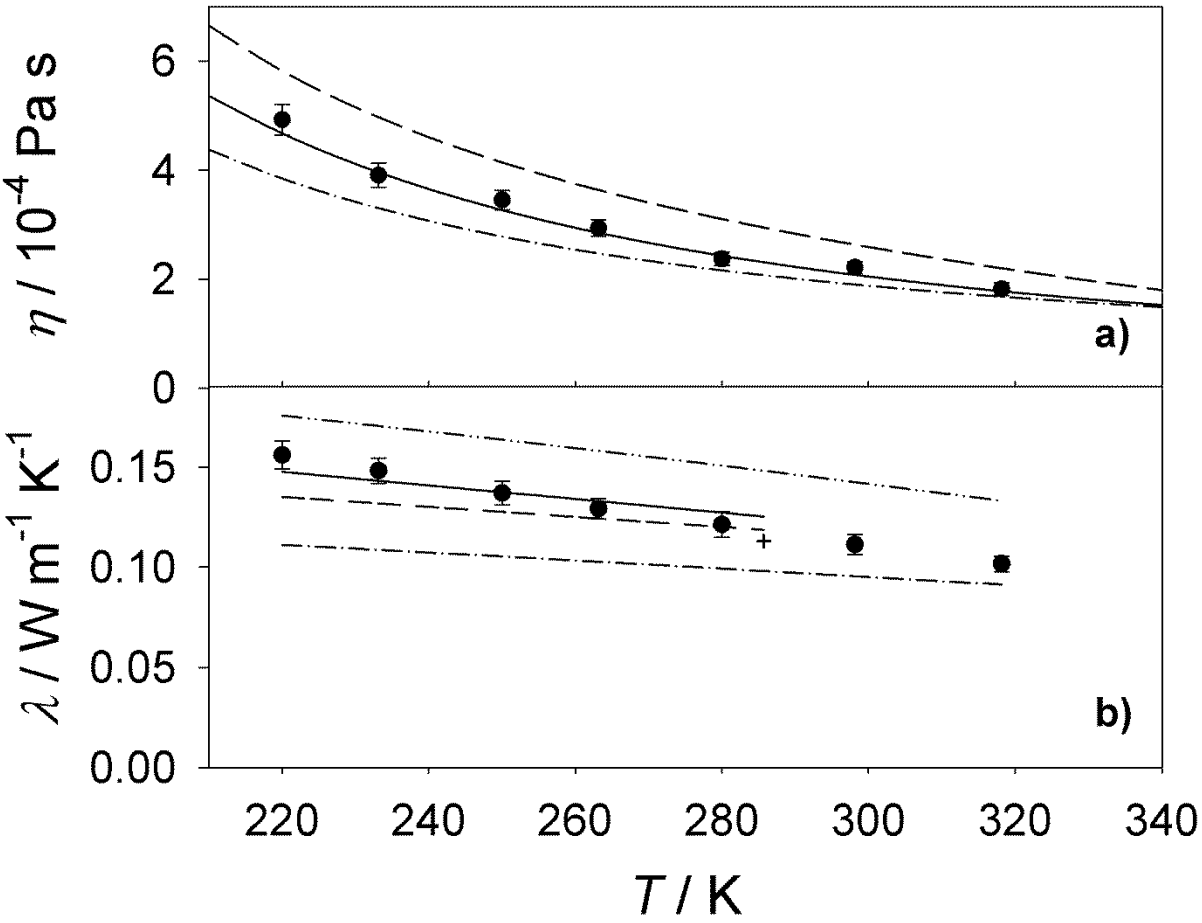
η / 10^-4 Pa s
6
4
2
0
a)
λ / W m^-1 K^-1
0.15
0.10
0.05
0.00
b)
220
240
260
280
300
320
340
T / K

Figure 14

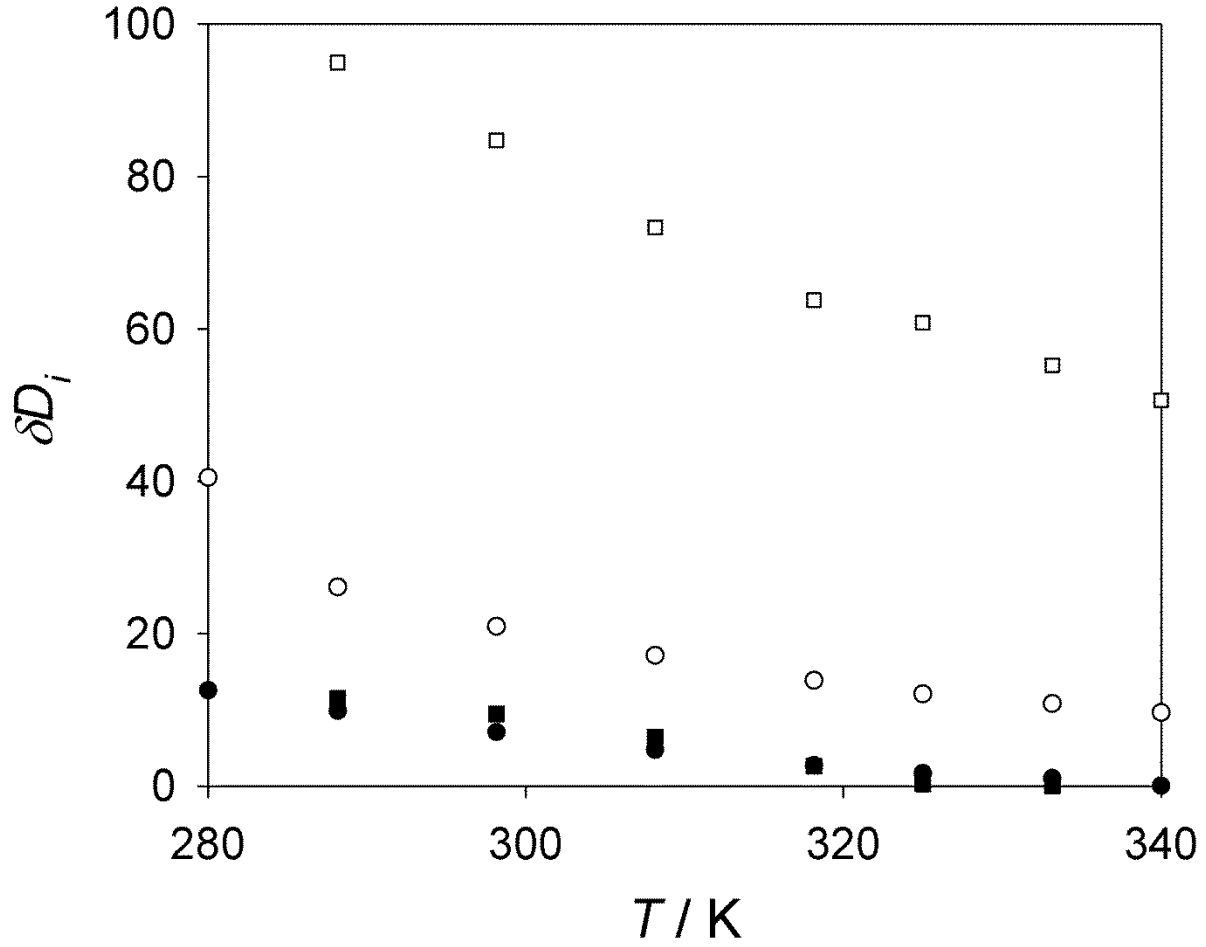

Figure 15.

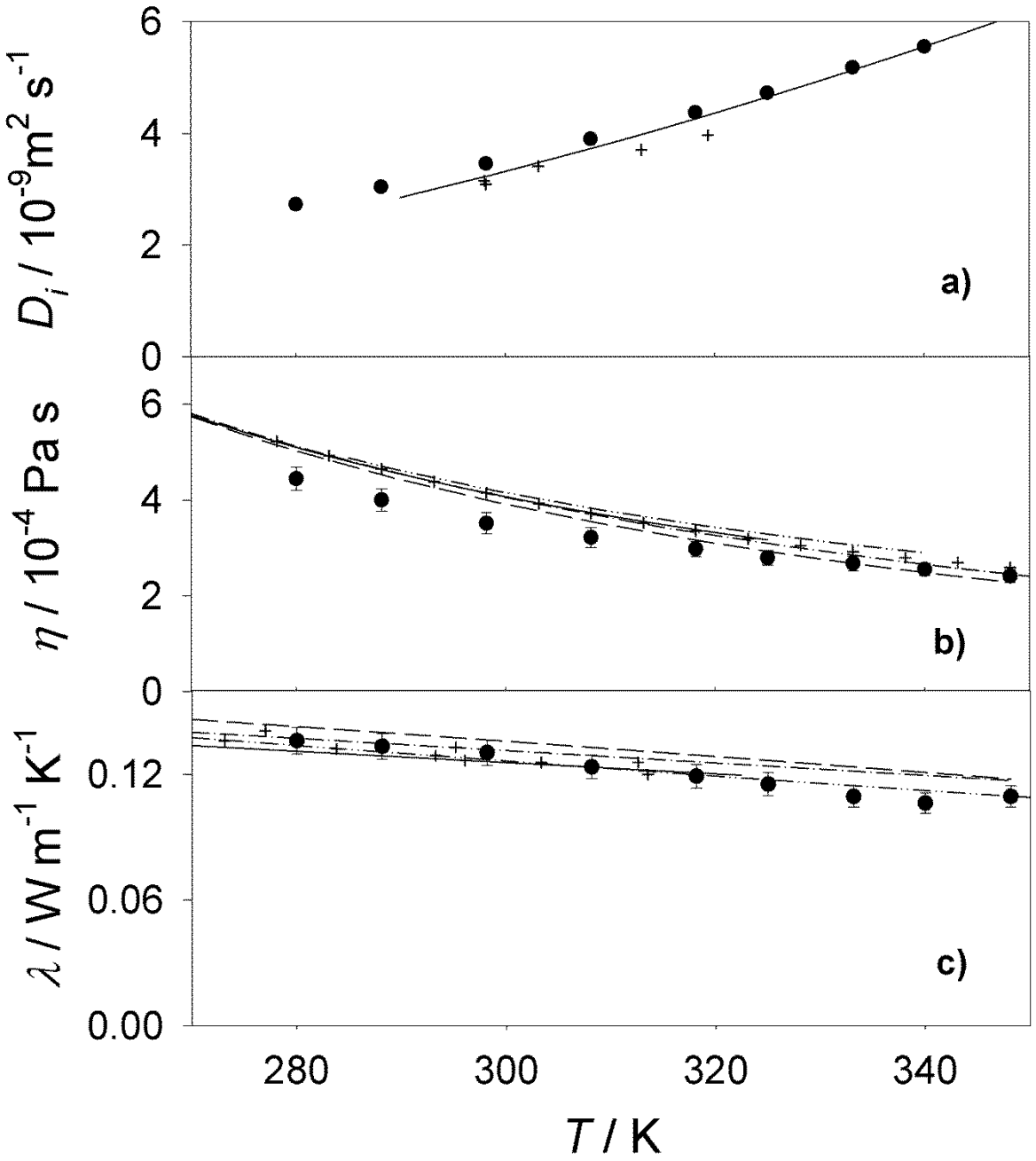
D_i / 10^{-9} m^2 s^{-1}
6
4
2
0
a)
η / 10^{-4} Pa s
6
4
2
0
b)
λ / W m^{-1} K^{-1}
0.12
0.06
0.00
c)
280
300
320
340
T / K

Figure 16.

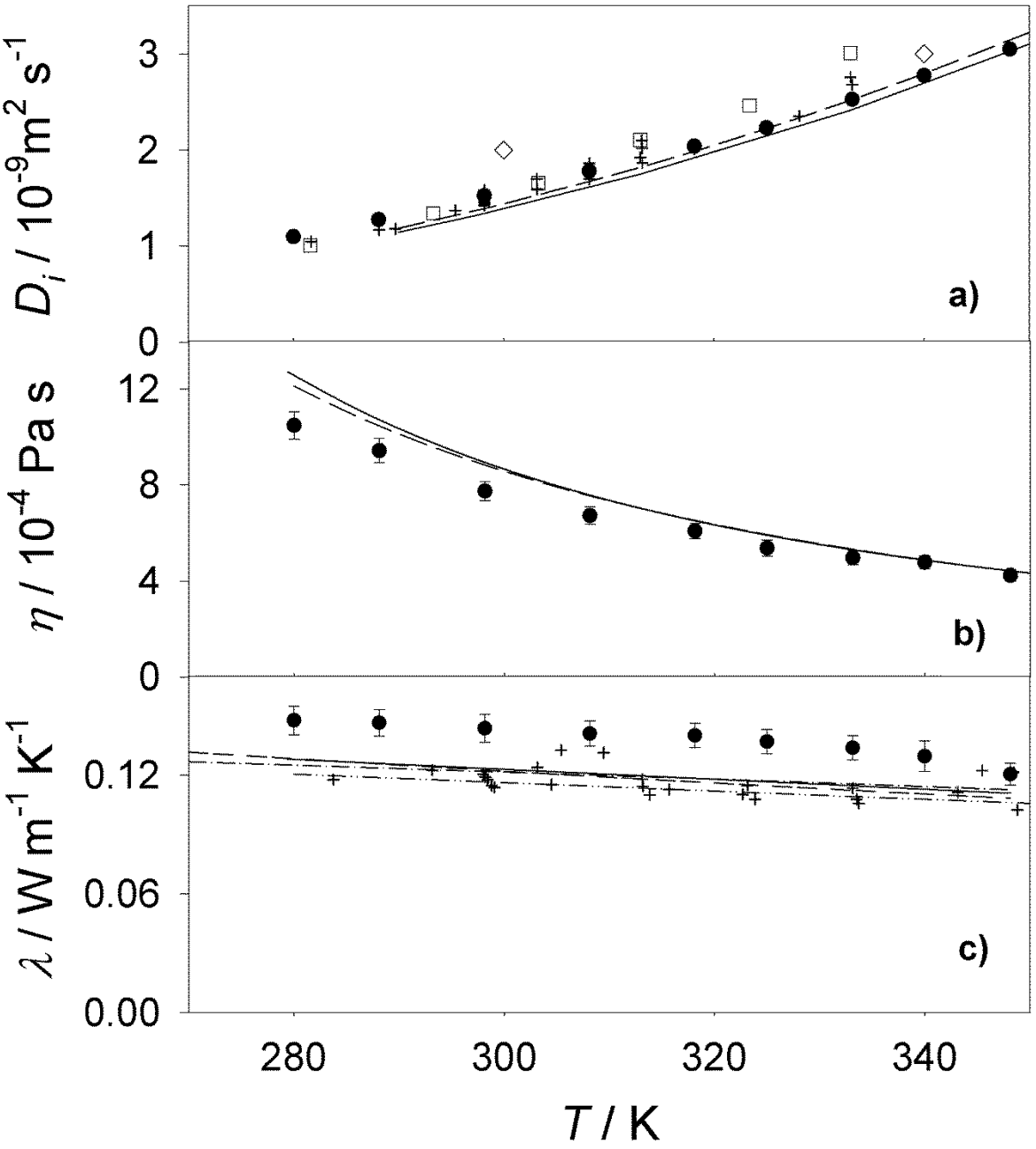
D_i / 10^{-9}m^2 s^{-1}
3
2
1
0
a)
η / 10^{-4} Pa s
12
8
4
0
b)
λ / W m^{-1} K^{-1}
0.12
0.06
0.00
c)
280
300
320
340
T / K

References

[1] Ford, D.C., Dubbeldam, D., Snurr, R.Q., Künzel, V., Wehring, M., Stallmach, F., Kärger, J., Müller, U., J. Phys. Chem. Lett. 3 (2012) 930-933.

[2] Vrabec, J., Stoll, J., Hasse, H., J. Phys. Chem. B 105 (2001) 12126-12133.

[3] Lísal, M., Nezbeda, I., Smith, W.R., J. Chem. Phys. 110 (1999) 8597-8604.

[4] Matar, S., Hatch, L.F., Chemistry of Petrochemical Processes. Second ed., Gulf Professional Publ., Butterworth-Heinemann, Woburn, Massachusetts, 2001.

[5] Yang, C., Fischer, L., Maranda, S., Worlitschek J., Energy Build. 87 (2015) 25-36.

[6] Besson, M., Gauthard, F., Horvath, B., Gallezot, P., J. Phys. Chem. B 109 (2005) 2461-2467.

[7] Rutkai, G., Thol, M., Lustig, R., Span, R., Vrabec, J., J. Chem. Phys. 139 (2013) 41102.

[8] Gedanitz, H., Davila, M.J., Lemmon, E.W., J. Chem. Eng. Data 60 (2015) 1331-1337.

[9] Zhou, Y., Liu, J., Penoncello, S.G., Lemmon, E.W., J. Phys. Ref. Data 43 (2014) 043105.

[10] Eckl, B., Vrabec, J., Hasse, H., J. Phys. Chem. B 112 (2008) 12710-12721.

[11] Windmann, T., Linnemann, M., Vrabec, J., J. Chem. Eng. Data 59 (2014) 28-38.

[12] Medina, J.S., Prosmiti, R., Villarreal, P., Delgado-Barrio, G., Winter, G., González, B., Alemán, J.V., Collado, C., Chem. Phys. 388 (2011) 9-18.

[13] Raabe, G., Sadus, R.J., J. Chem. Phys. 134 (2011) 234501.

[14] Lustig, R., Mol. Phys. 59 (1986) 173-194.

[15] Schuler, L.D., Daura, X., Van Gunsteren, W.F., J. Comput. Chem. 22 (2001) 1205-1218.

[16] Keasler, S.J., Charan, S.M., Wick, C.D., Economou, I.G., Siepmann, J.I., J. Phys. Chem. B 116 (2012) 11234-11246.

[17] Bourasseau, E., Ungerer, P., Boutin, A., J. Phys. Chem. B 106 (2002) 5483-5491.

[18] Neubauer, B., Boutin, A., Tavitian, B., Fuchs, A.H., Mol. Phys. 97 (1999) 769-776.

[19] Errington, J.R., Panagiotopoulos, A.Z., J. Chem. Phys. 111 (1999) 9731-9738.

[20] Hoheisel, C., Würflinger, A., J. Chem. Phys. 91 (1989) 473-476.

[21] Milano, G., Müller-Plathe, F., J. Phys. Chem. B 108 (2004) 7415-7423.

[22] Toxvaerd, S., J. Chem. Phys. 93 (1990) 4290-4295.

[23] Ungerer, P., Beauvais, C., Delhommelle, J., Boutin, A., Rousseau, B., Fuchs, A. H., J. Chem. Phys. 112 (2000) 5499-5510.

[24] Merker, T., Vrabec, J., Hasse H., Soft Mater. 10 (2012) 3-25.

[25] Wensink, E.J.W., Hoffmann, A.C., van Maaren, P.J., van der Spoel, D., J. Chem. Phys. 119 (2003) 7308-7317.

[26] Schmidt, M.W., Baldridge, K.K., Boatz, J.A., Elbert, S.T., Gordon, M.S., Jensen, J.H., Koseki, S., Matsunaga, N., Nguyen, K.A., Su, S., Windus, T.L., Dupuis, M., Montgomery, J.A., J. Com. Chem. 14 (1993) 1347-1363.

[27] Essén, H., Svensson, M., Comp. Chem. (Oxford, United Kingdom) 20 (1996) 389-395.

[28] Vrabec, J., Hasse, H., Mol. Phys. 100 (2002) 3375 □3383.

[29] Lin, D.C.K., Silberberg, I.H., McKetta, J.J., J. Chem. Eng. Data 15 (1970) 483-492.

[30] Rossini, F.D., Selected values of physical and thermodynamic properties of hydrocarbons and related compounds: comprising the tables of the American Petroleum Institute Research Project 44 extant as of December 31, 1952., Carnegie Press, Pittsburgh, 1953.

[31] David, H.G., Hamann, S.D., Thomas, R.B., Aust. J. Chem. 12 (1959) 309-318.

[32] Heisig, G.B., J. Am. Chem. Soc. 63 (1941) 1698-1699.

[33] Daubert, T., Danner, R.,API technical data book □petroleum Petroleum Institute (API), Washington, 1997

[34] Clapeyron, E.J., J. Ec. Polytech. (Paris) 23 (1834) 153-190.

[35] Willstätter, R., Bruce, J., Ber. Dtsch. Chem. Ges. 40 (1907) 3979-3999.

[36] Kaarsemaker, S.J., Coops, J., Recl. Trav. Chim. Pays-Bas 71 (1952) 261-276.

[37] Smith, B., Srivastava, R., Thermodynamic data for pure components, Elsevier, Amsterdam, 1986.

[38] McCullough, J.P., Pennington, R.E., Smith, J.C., Hossenlopp, I.A., Waddington, G., J. Am. Chem. Soc. 81 (1959) 5880-5883.

[39] Hugill, J.A., McGlashan, M.L., J. Chem. Thermodyn. 10 (1978) 95-100.

[40] Egloff, G., Physical constants of hydrocarbons, Reinhold Publishing Corp., New York, 1939.

[41] Young, S., Sci. Proc. R. Dublin Soc. 12 (1910), 374-443.

[42] Kerns, W., Anthony, R., Eubank, P., AIChE Symp. Ser. (1974) 14-21.

[43] Francis, A., Ind. Eng. Chem. 49 (1957) 1779-1786.

[44] Lenoir, J.M.,. A program of experimental measurements of enthalpies of binary hydrocarbons mixtures above 100 F and in the critical region, in Proceedings of the American Petroleum Institute 47, API, 1967, pp. 640-652.

[45] Thermodynamics Research Center, TRC Tables: Hydrocarbons. The Texas A&M University System: College Station, TX, 1990.

[46] Prengle, H.W., Felton, E.G., Pike, M.A., J. Chem. Eng. Data 12 (1967) 193-196.

[47] Green, M.S., J. Chem. Phys. 22 (1954) 398-413.

[48] NIST, 2013. Experimental geometry data (http://cccbdb.nist.gov/).

[49] Graham Solomons, T.W., Fryhle C.B., Organic Chemistry, Tenth ed., John Wiley & Sons., Hoboken, N.J., 2011.

[50] Morrison, R.T., Boyd, R.N., Organic chemistry, Fifth ed., Allyn and Bacon, Boston-Massachusetts, 1987.

[51] Bastiansen, O., Fernholt, L., Seip, H.M., Kambara, H., Kuchitsu, K., J. Mol. Struct. 18 (1973) 163-168.

[52] Rowley, R.L., Wilding, W.V., Oscarson, J. L., Yang, Y., Zundel, N.A., Daubert, T.E., Danner, R.P., The DIPPR data compilation of pure compound properties, AIChE, New York., 2007.

[53] Watson, K.M., Ind. Eng. Chem. 35 (1943) 398-406.

[54] Rackett, H.G., J. Chem. Eng. Data 15 (1970) 514-517.

[55] Merker, T., Vrabec, J., Hasse, H., Fluid Phase Equilib. 315 (2012) 77-83.

[56] Besnard, M., Dianoux, A.J., Lalanne, P., Lassegues, J.C., J. Phys. France 38 (1977) 1417-1422.

[57] Liessmann, G., Schmidt, W., Reiffarth S., Recommended Thermophysical Data; Data Compilation of the Sächsische Olefinwerke Böhlen, Germany, 1995.

[58] Yaws, C.L., Transport properties of chemicals and hydrocarbons. Viscosity, thermal conductivity and diffusivity of C1 to C100 organics and Ac to Zr inorganics., William Andrew Inc., N. Y, 2009.

[59] Yaws, C.L., Yaws' Handbook of Thermodynamic and Physical Properties of Chemical Compounds: physical, thermodynamic and transport properties for 5,000 organic chemical compounds. Knovel, Norwich, N. Y., 2003.

[60] Hopfe, D., Data Compilation of FIZ CHEMIE, Germany, 1990.

[61] Dysthe, D.K., Fuchs, A.H., Rousseau, B., J. Chem. Phys. 112 (2000) 7581-7590.

[62] Fischer, J., Weiss, A., Ber. Bunsen-Ges. Phys. Chem. 90 (1986) 896-905.

[63] Enninghorst, A., Wayne, F.D., Zeidler, M.D., Mol. Phys. 88 (1996) 437-452.

[64] Fishman, E., Vassillades, T., J. Phys. Chem. 63 (1959) 1217-1218.

[65] Holz, M., Weingartner, H., J. Magn. Res. 92 (1991) 115-125.

[66] Ma, R.-F., Shi, L., Duan, Y.-Y., Han, L.-Z., Liu, N.-X., J. Chem. Eng. Data 48 (2003) 1418-1421.

[67] Lemmon, E.W., Huber M.L., McLinden, M.O., REFPROP Reference Fluid Thermodynamic and Transport Properties, NIST Standard Reference Database 23 in: Technology, N.I.O.S.A. version 9.1, Gaithersburg, 2013.

[68] Assael, M.J., Dalaouti, N.K., Int. J. Thermophys. 22 (2001) 659-678.

[69] Watanabe, H., Kato, H., J. Chem. Eng. Data 49 (2004) 809-825.

[70] Ishkhanov, A.M., Grigor'ev, B.A., Pugach, V.V., Izv. Vyssh. Uchebn. Zaved., Neft' Gaz 24 (1981) 32-37.

[71] Huber, M.L., Laesecke, A., Perkins, R.A., I. Eng. Chem. Res. 42 (2003) 3163-3178.

[72] Freer, R., Sherwood, J.N., J. Chem. Soc., Faraday Trans. I, 76 (1980) 1030-1037.

[73] Holz M., Heil S.R., Sacco, A., Phys. Chem. Chem. Phys. 2 (2000) 4740-4742.

[74] Iwahashi, M., Kasahara, Y., J. Oleo Sci. 56 (2007) 443-448.

[75] Jonas, J., Hasha, D., Huang, S.G., J. Phys. Chem. 84 (1980) 109-112.

[76] Kessler, D., Witte, H., Weiss, A., Ber. Bunsen-Ges. Phys. Chem. 73 (1969) 368-376.

[77] Polzin, B., Weiss, A., Ber. Bunsen-Ges. Phys. Chem. 94 (1990), 746-758.

[78] O'Reilly, D.E., Peterson, E.M., Hogenboom, D.L., J. Chem. Phys. 57 (1972) 3969-3976.

[79] Brodka, A., Zerda, T.W., J. Chem. Phys. 97 (1992) 5669-5675.

[80] Mukherjee, A.K., Das T.R., J. Indian Ins. Sci. 67 (1987) 75-82.

[81] Naziev, Y.M., Gumbatov, A.M., Akhmedov, A.K., Abasov, A.A., Abasov, R.A., Izv. Vyssh. Uchebn. Zaved., Neft' Gaz 28 (1985), 57-61.

[82] Pugach, V.V., Izv. Vyssh. Uchebn. Zaved., Neft' Gaz 23 (1980) 48 □51.

[83] Rowley, R.L., Gubler, V., J. Chem. Eng. Data 33 (1988) 5-8.

[84] Sankarshana, T., Bhagavanth, R.M., Indian Chem. Eng. 31 (1989) 84 □89.

[85] Tanaka, Y., Hase, T., Kubota, H., Makita, T., Ber. Bunsen-Ges. Phys. Chem. 92 (1988), 770□776.

[86] Tarzimanov A.A., Izv. Vyssh. Uchebn. Zaved., Neft' Gaz 9 (1963) 75□79.

[87] Deublein, S., Eckl, B., Stoll, J., Lishchuk, S.V., Guevara□Carrion, G., Glass, C.W., Merker, T., Bernreuther, M., Hasse, H., Vrabec, J., Com. Phys. Comm. 182 (2011) 2350-2367.

[88] Allen, M. P., Tildesley, D.J., Computer simulation of liquids. Oxford University Press, N. Y., 1989.

[89] Lustig, R., Mol. Phys. 65 (1988) 175-179.

[90] Schoen, M., Hoheisel, C., Mol. Phys. 52 (1984) 33-56.

[91] Flyvbjerg, H., Petersen, H.G., J. of Chem. Phys. 91 (1989) 461-466.

Supplementary material to:

Lennard-Jones force field parameters for cyclic alkanes from cyclopropane to cyclohexane

Y. Mauricio Muñoz-Muñoz[a,b], Gabriela Guevara-Carrion[b], Mario Llano-Restrepo[a] , Jadran Vrabec*[b]

(a) School of Chemical Engineering, Universidad del Valle, Ciudad Universitaria Melendez, Building 336, Apartado 25360, Cali, Colombia; (b) Thermodynamics and Energy Technology, University of Paderborn, Warburger Straße 100, 33098 Paderborn, Germany.

Table 1. Vapor-liquid equilibria of cyclopropane. Simulation results (sim) are compared to the DIPPR correlation for the vapor pressure [1], to the Racket equation (RE) for the saturated liquid density [2], to Clausius-Clapeyron (CC) data for the saturated vapor density and to the Watson equation (WE) for the enthalpy of vaporization [3]. The number in parentheses indicates the statistical uncertainly in the last digit.

T K	p_{sim} MPa	p_{DIPPR} MPa	$\rho_{L,sim}$ mol l^{-1}	$\rho_{L,RE}$ mol l^{-1}	$\rho_{V,sim}$ mol l^{-1}	$\rho_{V,CC}$ mol l^{-1}	Δhv_{sim} kJ mol^{-1}	Δhv_{WE} kJ mol^{-1}
219	0.044(4)	0.0366	17.137(3)	17.2294	0.024(2)	0.0202	19.98(0)	21.0356
242	0.121(5)	0.1090	16.485(4)	16.5588	0.062(3)	0.0557	19.16(1)	20.0185
264	0.278(6)	0.2539	15.849(5)	15.8762	0.134(3)	0.1224	18.30(1)	18.9517
287	0.553(7)	0.5283	15.127(6)	15.1071	0.253(3)	0.2453	17.28(1)	17.7091
310	1.02 (1)	0.9803	14.351(8)	14.2610	0.455(4)	0.4489	16.06(1)	16.2893
333	1.69 (1)	1.6697	13.48 (1)	13.3021	0.752(5)	0.7748	14.60(1)	14.6082
355	2.62 (2)	2.6143	12.54 (2)	12.2107	1.198(7)	1.2706	12.85(2)	12.5946
363	2.99 (2)	3.0405	12.12 (2)	11.7441	1.384(8)	1.5210	12.12(3)	11.6993
370	3.47 (2)	3.4542	11.79 (2)	11.2874	1.671(8)	1.7865	11.29(3)	10.8021
378	3.90 (2)	3.9774	11.24 (3)	10.6823	1.91 (1)	2.1673	10.40(4)	9.5812

Table 2. Vapor-liquid equilibria of cyclobutane. Simulation results (sim) are compared to DIPPR correlations [1]. The number in parentheses indicates the statistical uncertainly in the last digit.

T K	p_{sim} MPa	p_{DIPPR} MPa	$\rho_{L,sim}$ mol l^{-1}	$\rho_{L,RE}$ mol l^{-1}	$\rho_{V,sim}$ mol l^{-1}	$\rho_{V,CC}$ moll^{-1}	Δhv_{sim} kJ mol^{-1}	Δhv_{WE} kJ mol^{-1}
252.96	0.030(4)	0.0256	13.126(3)	13.0403	0.015(2)	0.0123	24.75(1)	25.3772
268.15	0.058(5)	0.0508	12.849(3)	12.7955	0.026(2)	0.0232	24.16(1)	24.7371
293.15	0.138(5)	0.1322	12.373(4)	12.3702	0.059(2)	0.0566	23.13(1)	23.6196
298.15	0.169(7)	0.1567	12.276(4)	12.2813	0.071(3)	0.0663	22.89(1)	23.3838
350	0.68 (1)	0.6724	11.167(7)	11.2586	0.263(4)	0.2650	20.22(1)	20.5652
400	1.85 (1)	1.8983	9.88 (1)	9.9785	0.719(6)	0.7679	16.63(3)	16.6615
436.93	3.33 (2)	3.5381	8.59 (2)	8.5282	1.395(9)	1.6555	12.73(5)	11.7468
437	3.35 (2)	3.5417	8.56 (3)	8.5247	1.419(9)	1.6582	12.61(6)	11.7342

Table 3. Vapor-liquid equilibria of cyclopentane. Simulation results (sim) are compared to a reference equation of state [4]. The number in parentheses indicates the statistical uncertainly in the last digit.

T K	p_{sim} MPa	p_{DIPPR} MPa	$\rho_{L,sim}$ mol l^{-1}	$\rho_{L,RE}$ mol l^{-1}	$\rho_{V,sim}$ mol l^{-1}	$\rho_{V,CC}$ mol l^{-1}	Δhv_{sim} kJ mol^{-1}	Δhv_{WE} kJ mol^{-1}
279	0.019(4)	0.0187	10.796(2)	10.821	0.008(2)	0.008	28.96(1)	29.43
308	0.061(6)	0.0615	10.389(3)	10.415	0.024(2)	0.025	27.68(1)	28.03
337	0.174(6)	0.1552	9.977(3)	10.000	0.065(2)	0.058	26.28(1)	26.56
366	0.363(8)	0.6765	9.519(5)	9.008	0.130(3)	0.239	24.71(1)	22.79
395	0.695(9)	1.1877	9.034(6)	8.424	0.242(3)	0.424	22.91(2)	20.37
424	1.21 (1)	1.9416	8.480(8)	7.716	0.420(4)	0.735	20.72(2)	17.27
453	1.97 (1)	0.1599	7.83 (1)	9.985	0.709(5)	0.060	17.97(3)	26.51
482	2.94 (2)	3.0139	6.97 (3)	6.729	1.120(7)	1.325	14.49(6)	12.76

Table 4. Vapor-liquid equilibria of cyclohexane. Simulation results (sim) are compared to a reference equation of state [5]. The number in parentheses indicates the statistical uncertainly in the last digit.

T K	p_{sim} MPa	p_{DIPPR} MPa	$\rho_{L,sim}$ mol l^{-1}	$\rho_{L,RE}$ mol l^{-1}	$\rho_{V,sim}$ mol l^{-1}	$\rho_{V,CC}$ mol l^{-1}	Δhv_{sim} kJ mol^{-1}	Δhv_{WE} kJ mol^{-1}
336	0.059(6)	0.0573	8.722(3)	8.762	0.022(2)	0.021	31.02(1)	31.00
368	0.151(7)	0.1521	8.349(3)	8.376	0.052(3)	0.052	29.35(1)	29.16
399	0.333(7)	0.3301	7.968(4)	7.980	0.109(2)	0.109	27.52(2)	27.21
431	0.640(9)	0.6452	7.514(5)	7.536	0.204(3)	0.209	25.31(2)	24.90
462	1.12(1)	1.1229	7.049(8)	7.051	0.357(3)	0.368	22.82(3)	22.24
494	1.83(1)	1.8472	6.45(1)	6.446	0.601(4)	0.639	19.57(5)	18.74
526	2.90(2)	2.8716	5.72(4)	5.605	1.064(6)	1.146	15.08(9)	13.73

Table 5. Second virial coefficient of cyclopropane. Simulation results (sim) are compared to the DIPPR correlation [1].

T K	B_{sim} l mol^{-1}	B_{DIPPR} l mol^{-1}
225	-0.529	-0.7413
256	-0.408	-0.5435
300	-0.299	-0.3798
430	-0.143	-0.1742
710	-0.034	-0.0463
1195	0.022	0.01602
1595	0.040	0.03679
1993	0.049	0.0488

Table 6. Second virial coefficient of cyclobutane. Simulation results (sim) are compared to the DIPPR correlation [1].

T K	B_{sim} l mol^{-1}	B_{DIPPR} l mol^{-1}
240	-0.913	-1.15313
270	-0.701	-0.8452
350	-0.404	-0.4571
500	-0.186	-0.2045
730	-0.064	-0.0735
930	-0.015	-0.02308
1150	0.017	0.00915
1600	0.050	0.045
2290	0.073	0.071

Table 7. Second virial coefficient of cyclopentane. Simulation results (sim) are compared to the DIPPR correlation [1].

T K	B_{sim} l mol^{-1}	B_{DIPPR} l mol^{-1}
297.5	-0.9255	-1.0945
336	-0.6991	-0.7823
400	-0.4741	-0.5007
610	-0.1751	-0.1652
1010	-0.0127	-0.0098
1535	0.0554	0.05
2560	0.0996	0.0897

Table 8. Second virial coefficient of cyclohexane. Simulation results (sim) are compared to the DIPPR correlation [1].

T / K	B_{sim} / l mol^{-1}	B_{DIPPR} / l mol^{-1}
276.7	-1.710	-2.3016
300	-1.380	-1.7722
350	-0.942	-1.1083
400	-0.689	-0.7616
500	-0.411	-0.4228
1000	-0.032	-0.0339
1500	0.058	0.04805
2000	0.098	0.0841
2500	0.119	0.1045

Table 9. Density, self-diffusion coefficient, shear viscosity and thermal conductivity of cyclopropane. The number in parentheses indicates the statistical uncertainty in the last digit.

T / K	ρ / mol l^{-1}	D_i / 10^{-9} m^2 s^{-1}	η / 10^{-4} Pa s	λ / W m^{-1} K^{-1}
155	18.84	1.023(4)	7.2(3)	0.193(8)
170	18.45	1.520(3)	5.6(3)	0.185(8)
185	18.05	2.045(5)	4.2(2)	0.179(7)
200	17.67	2.764(5)	3.2(2)	0.167(6)
220	17.11	3.729(7)	2.6(1)	0.160(7)
250	16.27	5.648(8)	1.9(1)	0.143(6)
280	15.35	8.190(9)	1.52(9)	0.115(5)
298.15	14.75	10.26(1)	1.32(9)	0.103(4)
318.15	14.02	12.67(5)	1.11(8)	0.095(4)

Table 10. Density, self-diffusion coefficient, shear viscosity and thermal conductivity of cyclobutane. The number in parentheses indicates the statistical uncertainty in the last digit.

T / K	ρ / mol l^{-1}	D_i / 10^{-9} m^2 s^{-1}	η / 10^{-4} Pa s	λ / W m^{-1} K^{-1}
220	13.72	2.175(8)	4.9(3)	0.154(7)
233.15	13.49	2.670(7)	3.9(2)	0.148(6)
250	13.18	3.394(6)	3.5(2)	0.137(6)
263.15	12.95	4.023(7)	2.9(1)	0.129(5)
280	12.63	4.944(8)	2.4(1)	0.121(7)
298.15	12.28	6.022(9)	2.2(1)	0.111(5)
318.15	11.87	7.46(1)	1.8(1)	0.102(3)

Table 11. Density, self-diffusion coefficient, shear viscosity and thermal conductivity of cyclopentane. The number in parentheses indicates the statistical uncertainty in the last digit.

T	ρ	D_i	η	λ
K	mol l^{-1}	10^{-9} m^2 s^{-1}	10^{-4} Pa s	W m^{-1} K^{-1}
280	10.86	2.733(6)	4.4(2)	0.136(7)
288.15	10.74	3.045(7)	4.0(2)	0.133(6)
298.15	10.60	3.462(7)	3.5(2)	0.130(6)
308.15	10.45	3.903(8)	3.2(2)	0.123(6)
318.15	10.29	4.374(7)	3.0(2)	0.119(6)
325	10.18	4.726(8)	2.8(1)	0.115(6)
333.15	10.06	5.182(8)	2.7(2)	0.110(5)
340	9.95	5.556(8)	2.5(1)	0.106(5)
348.15	9.82	6.04(1)	2.4(1)	0.110(5)

Table 12. Density, self-diffusion coefficient, shear viscosity and thermal conductivity of cyclohexane. The number in parentheses indicates the statistical uncertainty in the last digit.

T	ρ	D_i	η	λ
K	mol l^{-1}	10^{-9} m^2 s^{-1}	10^{-4} Pa s	W m^{-1} K^{-1}
280	9.43	1.097(3)	10.5(6)	0.148(7)
288.15	9.33	1.275(4)	9.4(5)	0.147(7)
298.15	9.22	1.524(4)	7.7(4)	0.143(7)
308.15	9.10	1.781(5)	6.7(4)	0.141(6)
318.15	8.98	2.040(4)	6.1(3)	0.140(6)
325	8.90	2.230(6)	5.4(3)	0.137(6)
333.15	8.80	2.527(6)	5.0(3)	0.133(6)
340	8.72	2.777(6)	4.8(3)	0.130(6)
348.15	8.62	3.050(7)	4.2(2)	0.121(6)

References

[1] Rowley, R.L., Wilding, W.V., Oscarson, J. L., Yang, Y., Zundel, N.A., Daubert, T.E., Danner, R.P., 2007. The DIPPR data compilation of pure compound properties., in: Properties, D.I.f.P. (Ed.). AIChE, New York.

[2] Rackett, H.G., 1970. Equation of state for saturated liquids. Journal of Chemical & Engineering Data 15, 514–517.

[3] Watson, K.M., 1943. Thermodynamics of the Liquid State. Industrial & Engineering Chemistry 35, 398–406.

[4] Gedanitz, H., Davila, M.J., Lemmon, E.W., 2013. Helmholtz equation of state for cyclopentane, unpublished.

[5] Zhou, Y., Liu, J., Penoncello, S.G., Lemmon, E.W., 2014. An equation of state for the thermodynamic properties of cyclohexane. Journal of Physical and Chemical Reference Data 43, 043105.